TAMPEREEN TEKNILLINEN YLIOPISTO
TAMPERE UNIVERSITY OF TECHNOLOGY

ANTTI SAARELA

ADVANCED ION BEAM SPUTTERING COATINGS FOR HIGH-POWER SEMICONDUCTOR DIODE LASERS

Master of Science Thesis

Examiners:
Prof. Mircea Guina and
PhD Jukka Viheriälä
The examiners and topic
approved on 31st January 2018

ABSTRACT

SAARELA, ANTTI: Advanced ion beam sputtering coatings for high-power semiconductor diode lasers
Tampere University of technology
Master of Science Thesis, 51 pages
June 2018
Master's Degree Programme in Science and Engineering
Major: Advanced Engineering Physics
Examiners: Professor Mircea Guina and Dr. Tech. Jukka Viheriälä

Keywords: semiconductor laser, diode laser, edge-emitting diode laser, cleaning, passivation, passivation layer, coating

High-power semiconductor diode lasers are widely used in industrial applications such as material processing and as pump lasers. One challenge in the development of these lasers is that the laser diode suffers sudden failures due to high optical power density at the facets of the laser. These failures occur due to surface states that permit the absorption or non-radiative recombination at the semiconductor-coating interface, in the coating itself or in the semiconductor lattice near the interface. Impurities or lattice defects near the facets often limit the maximum optical output power produced by a laser diode as well as limits the life time of the device.

Dielectric coatings are used to tailor the reflectivities of the laser diode facets. Ion beam sputtering is a method of depositing these coatings with the use of ion sources. Deposition parameters of the ion source affect the film quality and properties. Ion beams can also be used to pre-clean the semiconductor surface and to deposit different passivation layers prior to the coating. Appropriate treating of the laser facets, notably the output facet of the laser, can be used to not only increase the tolerance for high intensities but also increase the life time of the laser device.

In this thesis an assist source of an ion beam sputter was parametrized to produce different cleaning and passivation treatments. The treated devices were then tested with under pulsed operation to test the effectiveness of the treatments. Figure of merit for testing was the threshold of optical peak power where the devices experience sudden failure. Deposition parameters of aluminum oxide were found to have a significant effect on the damage threshold of the laser later in the thesis. Assist source was parametrized to produce uniform and controlled etching for the cleaning treatments. Assist source was also used to produce silicon nitride passivation layers using ion assisted deposition. Different cleaning treatments and passivation layers were applied to laser diodes.

Best devices showed an increase of 9 % on average damage threshold. Overall, the device performance, including devices with no applied treatments, was noticed to be notably weaker than commercially coated samples. After parametrization of primary source deposition parameters for aluminum oxide, the average COD threshold was found to increase by at least 50 %.

TIIVISTELMÄ

SAARELA, ANTTI: Ionisädesputterointipinnoitukset korkean tehon puolijohdediodilasereille
Tampereen teknillinen yliopisto
Diplomityö, 51 sivua
Kesäkuu 2018
Teknis-luonnontieteellinen diplomi-insinöörin tutkinto-ohjelma
Pääaine: Teknillinen fysiikka
Tarkastajat: Prof. Mircea Guina ja TkT Jukka Viheriälä

Avainsanat: puolijohdelaser, diodilaseri, reunaemittoiva diodilaseri, puhdistus, passivointi, passivointikerros, pinnoitus

Korkean tehon puolijohdediodelasereita käytetään laajalti teollisuuden sovellutuksissa sekä pumppulasereina. Yksi haaste näiden lasereiden kehityksessä on laserien ennenaikainen ja äkillinen hajoaminen laserin peilipinnoilla liian isoista valotehoista johtuen. Tämäntyyppiset hajoamiset voidaan yleensä selittää puolijohderakenteen ja pinnoituksen välissä tai välittömässä läheisyydessä olevilla pintatiloilla, jotka voivat rekombinoitua emittoimatta valoa tai absorboida sitä. Valoa absorboivat epäpuhtaudet tai kidevirheet rajoittavat usein laserin tuottamaa optista maksimitehoa lyhentäen myös laserien elinikää.

Dielektriohutkalvopinnoituksia käytetään lasereissa säätämään laserin kaviteetin pintojen heijastuvuuksia. Ionisädesputterointi on ohutkalvopinnoitteiden tekemiseen tarkoitettu laite ja tuotantotapa, jossa pinnoitukseen käytettävä materiaali irroitetaan ionisäteiden avulla. Käytetyt pinnoitusparametrit vaikuttavat merkittävästi tuotettujen ohutkalvojen laatuun ja ominaisuuksiin. Ionisäteitä voidaan myös käyttää puolijohdepintojen esipuhdistukseen sekä erilaisten passivointikerrosten pinnoitukseen. Oikeanlainen esikäsittely etenkin laserin tuottaman valon ulostulopinnalla lisää lasereiden kestämää maksimitehoa sekä pidentää niiden elinikää.

Tässä opinnäytetyössä tutkittiin ionisädesputterointilaitteen apuionilähteellä tuotettuja puhdistus- ja passivointikäsittelyjä. Apuionilähteelle etsittiin puhdistusparametrit, joilla pinnan etsaus oli kontrolloitua ja tasaista. Tämän lisäksi apuionilähteelle etsittiin parametrit passivointiin tarkoitettujen piinitridikerroksien tekemiseen. Käsiteltyjen laserien valotehon kesto mitattiin käyttämällä niitä pulssitetusti nousevalla virralla, kunnes ne hajosivat. Myös pääionilähteen vaikutusta lasereiden tehonkestävyyteen tutkittiin muuttamalla alumiinioksidin pinnoitusparametreja.

Paras käsittely lasereille tuotti 9 %:in nousun laserien hajoamistehon keskiarvossa. Käsitellyistä lasereista sekä myös käsittelemättömistä referenssilasereista huomattiin, että niiden tehonkesto on merkittävästi heikompi kuin lasereiden, jotka olivat kaupallisesti pinnoitettuja. Tästä syystä tutkittiin alumiinioksidin kasvatusparametrien vaikutusta laserien valotehon kestoon. Kasvatusparametreja optimoimalla saavutettiin ainakin 50 %:in lisäys käsittelemättömien lasereiden tehonkestoon.

PREFACE

This thesis was carried out at Laboratory of Photonics, Optoelectronics Research Centre in collaboration with Modulight. I would like to express my sincerest gratitude to the head of ORC, Prof. Mircea Guina, as well as Seppo Orsila and Dr. Petteri Uusimaa from Modulight, who have bestowed this opportunity upon me.

I would like to thank my supervisors Prof. Mircea Guina and Dr. Jukka Viheriälä for providing insightful assistance, encouragement and direction of this thesis. Especially I want to thank Dr. Lasse Orsila, who tirelessly provided guidance, insight and exceptional thin film knowledge in both the minor and major hurdles along the way.

I am thankful for my colleagues in ORC and Modulight. It is truly inspiring to work in welcoming communities filled with talent. Special thanks to Ville Vilokkinen and Petri Melanen for their unmatched semiconductor knowledge and the help they provided. I am thankful to Kirsi Rantala, Anu Vilokkinen and Marjut Hillberg for the guidance regarding the cleanroom work. I also thank Jarno Reuna for readily assisting me with equipment and machines used in this thesis as well as Dr. Jari Nikkinen and Dr. Soile Suomalainen for their valuable discussions regarding semiconductors and lasers.

I am grateful to all my friends in TUT, who have throughout my studies provided the ever necessary peer support. The late evenings studying for tests, calculating lengthy physical problems and writing lab reports would have been much grimmer without these amazing people tackling these problems along me. I would like to extend a special thank you to an excellent studying partner and former colleague Lauri Hytönen.

Lastly, I’d like to thank my family for their unconditional support throughout my whole life. I extend my thanks to Marikki for supporting me during this thesis. Thank you for believing in me and being there.

Tampere, June 8th, 2018

Antti Saarela

CONTENTS

1. INTRODUCTION 1
2. SEMICONDUCTOR LASERS 4
   2.1 Semiconductors 4
   2.2 Semiconductor junctions 6
   2.3 Optoelectronic devices 8
   2.4 Semiconductor lasers 11
3. OPTICAL THIN FILMS 15
   3.1 Fundamental properties 15
   3.2 Anti-reflective coatings 16
   3.3 High reflective coatings 17
   3.4 Adhesion and abrasion 23
4. ION BEAM SPUTTERING 25
   4.1 Basic properties 25
   4.2 Facet cleaning 29
   4.3 Catastrophic optical damage 31
   4.4 Semiconductor laser diode life time 33
5. RESULTS AND ANALYSIS 35
   5.1 Parametrization of the assist source 35
   5.2 Testing of surface treatments 39
   5.3 Effect of primary source deposition parameters 42
   5.4 Future possibilities 44
6. CONCLUSIONS 46
REFERENCES 47

LIST OF SYMBOLS AND ABBREVIATIONS

AR	Anti-reflective
BJT	Bipolar Junction Transistor
COD	Catastrophic Optical Damage
COMD	Catastrophic Optical Mirror Damage
DBR	Distributed Bragg Reflector
DFB	Distributed Feedback
FET	Field-Effect Transistor
HR	High reflective
IAD	Ion Assisted Deposition
IBS	Ion Beam Sputtering
IR	Infrared
LASER	Light Amplification by Stimulated Emission of Radiation
LED	Light Emitting Diode
MBE	Molecular Beam Epitaxy
MOCVD	Metalorganic Chemical Vapour Phase Epitaxy
QW	Quantum Well
RF	Radio Frequency
SCH	Separate Confinement Heterostructure
TE	Transverse Electric
TM	Transverse Magnetic
VCSEL	Vertical-Cavity Surface-Emitting Laser
VECSEL	Vertical External-Cavity Surface-Emitting Laser

α_i	losses in optical cavity
γ	gain coefficient
Γ_{QW}	confinement factor for a single quantum well
θ_l	angle of incidence for light
λ	wavelength
ν	frequency of light
Φ_l	phase shift of light in a layer

A_0	light component moving right in outer medium in matrix formalism
A_s	light component in substrate moving right in matrix formalism
B_0	light component moving left in outer medium in matrix formalism
B_s	light component in substrate moving left in matrix formalism
d_l	physical thickness of a layer
D_l	interface matrix for a layer
$D_{l,H}$	interface matrix for a high index layer
$D_{l,L}$	interface matrix for a low index layer
$D_{l,o}$	interface matrix for outer medium
$D_{l,p-p}$	interface matrix for p-polarized light in a layer
$D_{l,s}$	interface matrix for substrate
$D_{l,s-s}$	interface matrix for s-polarized light in a layer
E_F	energy of Fermi level
g	DBR's centre wavelengths relation to wavelength
h	Planck's constant

J_T	transparency current
J_{th}	threshold current density
L_c	length of laser cavity
m	mass
M	transfer matrix
M_{11}	component of transfer matrix
M_{12}	component of transfer matrix
M_{21}	component of transfer matrix
M_{22}	component of transfer matrix
n, n_1, n_2	refractive index
N	number of low and high index pairs in a DBR
n_e	electron density
n_f	refractive index of a film
n_H	refractive index of a high index layer
n_L	refractive index of a low index layer
$n_l(\lambda)$	wavelength dependent refractive index of a layer
n_o	refractive index of outer medium
N_{QW}	number of quantum wells
n_s	refractive index of a substrate
P_{DBR}	propagation matrix for a DBR layer
P_l	propagation matrix in a layer
R, R_1, R_2	reflectivity

1. INTRODUCTION

Ever since the demonstration of semiconductor laser diode [1], these light sources have been an expanding field reaching multibillion USD markets. As semiconductor lasers reach higher powers, become more efficient and meet even stricter spectral requirements, new markets are ready to be influenced. At the moment semiconductor lasers are widely used in optical storage, industrial applications and communications. Other notable fields are medicine, sensors, military applications and display systems.

Edge-emitting laser diodes are fabricated using epitaxial semiconductor layers grown on top of a semiconductor substrate wafer. This means that the epitaxially grown semiconductor layers, also called epilayers, follow the crystal pattern of the previous layer. Methods of controllably and accurately producing these include molecular beam epitaxy (MBE) and metalorganic chemical vapour phase epitaxy (MOCVD). These laser wafers then undergo fabrication steps including lithography, metallization and cleaving until they are laser bars. The laser devices are often coated as bars and then cleaved into chips. Laser bars can be seen in Fig. 1.

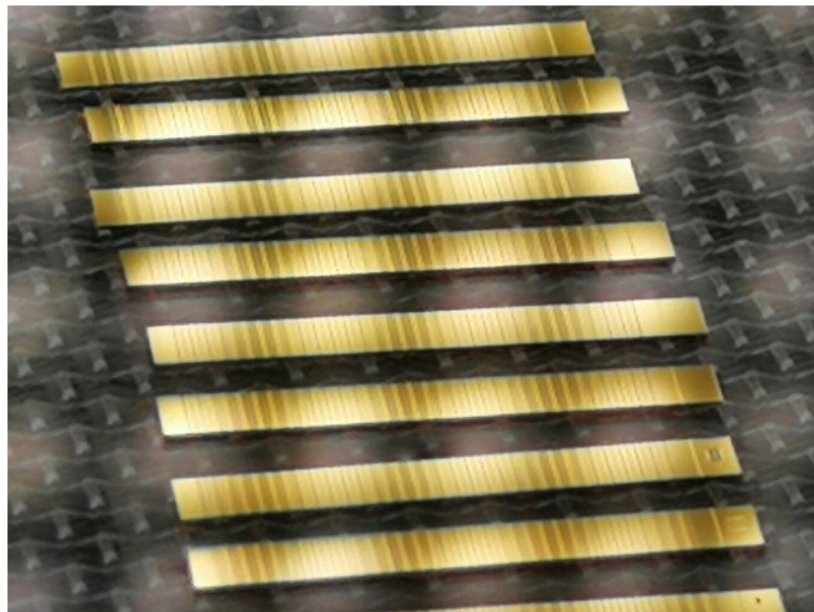

Figure 1. *Laser bars in a gel pack. Bars are usually 10 mm wide, 0.5–4 mm long and contains over 20 individual chips. Image is courtesy of Modulight Inc.*

Constant trend in semiconductor lasers is ever decreasing size. Thus one challenge in the development of these lasers is the increasing optical power density. Too high optical power generally leads to sudden device failures at the output. This catastrophic optical damage (COD) breaks the laser. The threshold for COD lowers as the device ages and is exposed to heating, ultimately leading to permanent failure of the laser chip. Lasers operated at higher powers are commonly more prone to failures due to high optical power density and high operating temperatures, shortening the laser's lifetime.

COD is ultimately caused by absorption in the semiconductor structure of the laser or at its resonator. An ideal mirror of a semiconductor laser does not absorb at all. However, semiconductors oxidize quickly and these oxides can generate unwanted surface states near the laser mirrors. At high operating powers these oxides or other impurities absorb some of the light emitted by the laser as well as cause non-radiative recombination, resulting in local heating and eventually the failure of the laser device due to COD.

Semiconductor laser facets, which form the optical resonator of the laser, require specific reflectivities for the laser to perform optimally. Because of this laser facets are almost always coated to achieve desired reflectivities. One technique these coatings can be deposited with is called ion beam sputtering (IBS). It involves an ion source where ions are generated and then accelerated towards a material target. These accelerated ions then knock atoms off of the material target that form a layer on the devices to be coated. This technique provides a controllable method of depositing thin films.

An important benefit of ion beam sputtering, introduced in chapter 4, is that the film can altered by a secondary ion source. Effects on the use of secondary assist source was systematically studied as early as 1963 by Donald Mattox and his coworkers [2]. This secondary ion source can be used to affect properties of the film during deposition or to clean the semiconductor laser facet prior to coating. When the cleaning is done in a controllable manner using ions of the right energy, oxides and other surface impurities can be removed without harming the semiconductor structure underneath increasing the laser's threshold for COD.

The process of cleaning and coating semiconductor lasers has to happen without intermediate removal of the devices from vacuum. This is because exposure to ambient air and the oxygen in it causes the surface to reoxidize. Reoxidation happens to some degree during the coating process as well as oxygen is present as sputtering atoms from the ion source or as a background gas. This is because dielectric mirrors are often compounds of oxygen. This problem can be alleviated through an introduction of a passivation layer. This layer is a thin and inert layer whose purpose is to prevent further reaction of the semiconductor material, thus passivating it.

Effectiveness of cleaning and passivation treatments prior to coating can be evaluated by measuring the COD levels of given devices. It is important to note that COD levels have

a certain amount of randomness in them, requiring a statistical approach. This is because even the slightest contamination in critical location or local defects in the semiconductor structure can cause the COD to happen at different optical power on seemingly identical chips. The laser chips are visually inspected to guarantee that the tested chips are of adequate quality.

The aim of this thesis is to find out suitable parameters for an IBS coater assist source to determine the effect of ion source coil power and positive voltage to etching speed and to have an initial parametrization to use the assist source. Different cleaning and passivation treatments can then be tested prior to coating for laser diodes. Then the laser devices of sufficient quality from each coating are tested under pulsed operation to determine the effect of cleaning and passivation treatments to the COD threshold.

This thesis consists of six chapters. In chapter 2 the basics of semiconductors, lasing and related physical phenomena are explained. Also important semiconductor devices are introduced. Optical thin films such as anti-reflective and high reflective coatings and their properties are addressed in chapter 3. Chapter 4 focuses on thin film deposition method IBS and possibilities it can add to the coating procedure such as different cleaning and passivation treatments. In this chapter is also explained COD as a phenomenon and semiconductor laser diode life time. Lastly, chapter 5 is reserved for results and analysis, and chapter 6 is for conclusions.

2. SEMICONDUCTOR LASERS

2.1 Semiconductors

Semiconductors have revolutionized the world. One event that could be considered to have started the revolution was when Michael Faraday found out that the resistance of silver sulfide decreased with the increase of temperature [3]. This sparked interest to this new kind of material and lead to discovery of more of semiconductor properties such as rectification, photoconductivity and photovoltaic effect [4].

Semiconductors are materials that consist of a crystalline structure. This means that the same fundamental building block is repeated to form the structure [5]. This building block is a cube and it's called a unit cell. The size of this cube is determined as lattice constant and it is the length of the cube's side. The simplest lattice structure is called simple cubic, which has a center of an atom in every corner of the lattice cube. More complex variations of this are the body-centered cubic and the face-centered cubic which have atoms in center of the cube or the faces of the cube, respectively. Important lattices in the field of semiconductor lasers are diamond lattice in silicon and zinc-blende in GaAs and InP [6]. Elemental semiconductors often have a diamond lattice structure and compound semiconductors generally have zinc-blende lattice [5].

Semiconductors used in industry are often doped to achieve the desired electrical properties. Doping means that impurities, atoms of a different material, are introduced to the lattice. The undoped semiconductor is called an intrinsic semiconductor, while the semiconductor that is used for doping is called a dopant. For doping to have a purpose, the dopant has to be of a different group in the periodic table of elements. This way the dopant will have a different number of valence electrons and thus add either excess electrons or holes. Holes are slots where an electron could reside, to the lattice. Whether electrons or holes, negative or positive charge carriers, are doped into the semiconductor, the result will be n-type or p-type extrinsic semiconductor, respectively [5]. A dopant that adds excess electrons to the lattice is called a donor and a dopant that adds holes is called an acceptor.

The reason semiconductors show unique electrical behavior can be seen in the energy band. To first understand the meaning of the electric bands and how they can be affected by doping, one must first understand an important concept called Fermi energy. Fermi energy is the energy of the highest manned state in a system occupied by fermions at a temperature of absolute zero [5]. Fermi energy is given as

$$E_F = \left(\frac{h^2}{8m}\right)\left(\frac{3}{\pi}\right)^{2/3} n_e^{2/3}, \tag{1}$$

where h is Planck's constant, m is the mass of a particle and n_e is the electron density. It is important to remember that this holds true only for particles called fermions, such as electrons, which behave in a way that a state can only be empty or occupied by a single particle. Consequently, Fermi energy is dependent on the electron density of the material and thus tailorable with doping.

Metals are highly conductive as they have a valence band and a conduction band close to each other or even overlapping. This means that there are always electrons and holes available to freely move and conduct electricity. In an intrinsic semiconductor thus energy gap between conduction and valence band, consequently called the band gap, is still relatively small. This allows some electrons to thermally excite to the conduction band and conduct electricity. On the other hand, in an insulator the band gap is large enough to prevent the excitation of electrons to the conduction band under normal circumstances. The band gap itself has no occupiable states and is not an allowed state for an electron. These band structures are demonstrated in Fig. 2.

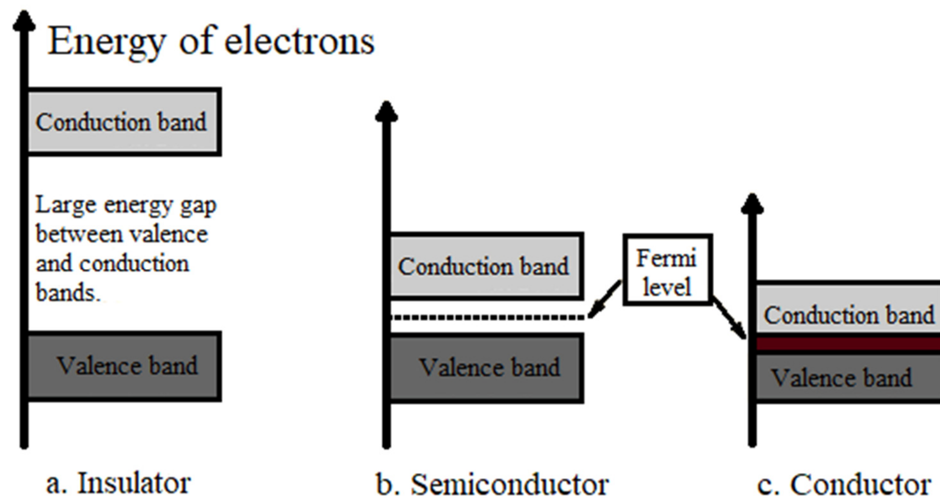

Figure 2. *Energy bands of an insulator, semiconductor and conductor. The dark red region in the energy bands of conductor represents the overlap of bands.*

The energy bands demonstrated above are not truly continuous allowed values for all the electrons in a system but a simplified demonstration. In reality, each electron with a different orbital location has a limited number of discrete allowed states [7]. Transitions between these states require energy if the transition is made to a state of higher energy than the original. In contrast, energy is released when a transition is made to state of a lower energy. These transitions between states are tied to absorption or emission of photon or phonon. The energy bands are also located in a wavenumber space, which repre-

sents the momentum of charge carriers. If a transition happens within the same wavenumber, only photon is emitted or absorbed. However, if the transition between states involves a shift in wavenumber as well, absorption or emission of a phonon is required for the transition. Band gap within the same wavenumber is called a direct bandgap while a band gap between different wavenumbers is called an indirect band gap.

2.2 Semiconductor junctions

To take full advantage of semiconductor properties and build the devices modern electronics rely on, semiconductor materials need to be arranged in a specific way. When the p and n doped materials are allowed to contact, the remarkable p-n junction is formed. This junction and its significance was ironically found in 1940 in an attempt to produce pure silicon Russell Ohl [8].

A p-n junction consists of three regions: positively doped p-side, negatively doped n-side and a depletion region in between. Majority carriers in p-side are holes while in the n-side they are electrons. Depletion region forms when the differently doped sides are placed in contact as the excess electrons from the n-side try to move to the p-side to balance out the electrical potential. Some of these electrons are able to diffuse to the p-side to fill a hole and form a negative ion leaving a positive ion behind to the n-side. [8] Width of the depletion region is dependent on the level of doping and is very often asymmetric [9]. Forming of the depletion region is demonstrated in Fig. 3.

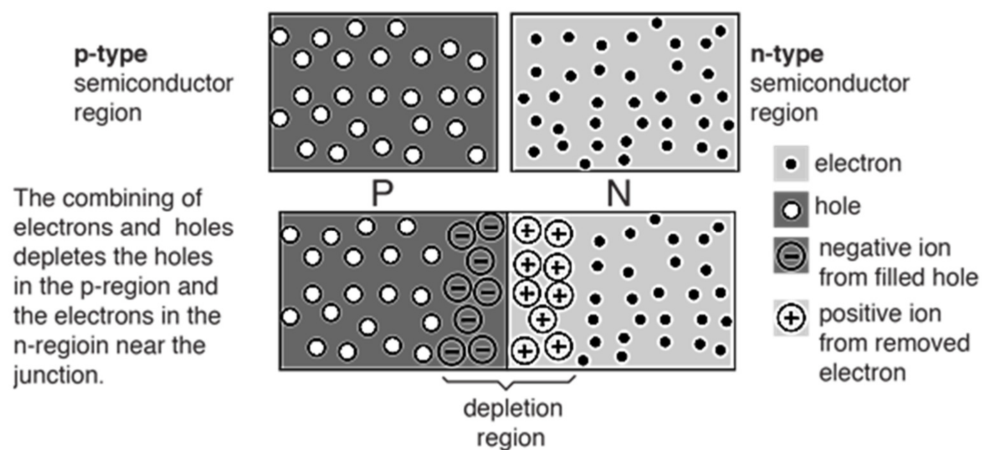

Figure 3. *Depletion region forms to the junction of two differently doped semiconductor materials as they are brought to contact* [10].

p-n junction is a diode [11]. This means that it has the capability of permitting current flow in one direction and blocking it in the other. Current flow is possible when the junction is biased in such a way that the p-side is connected to a higher voltage in comparison to the n-side. This condition is called a forward bias. In forward bias both sides' majority carriers will move towards the depletion region, narrowing it. If the p-side is connected

to a lower voltage than the n-side, the junction is reversely biased. The current flow is prevented from the n-side to the p-side in reverse bias as the majority carriers on both sides are pulled away from the depletion region, widening it and increasing its insulating capabilities [11].

Current flow in a p-n junction is a sum of two different currents: drift and diffusion current. Drift current is caused by the electric field in the depletion region and results in a current flow from n-side to p-side. Diffusion current is caused by a concentration difference in charge carriers. This causes, as the name suggests, diffusion of charge carriers from one side to another. Diffusion current can flow in both directions but is also affected by depletion region width [12]. The current-voltage graph of a p-n junction is shown in Fig. 4. Current flow in reverse bias is mainly caused by drift current and in forward bias the dominating current is diffusion current. In reverse bias the negative current is almost a constant until the breakdown region as the amount of minority carriers entering the depletion region is relatively unaffected by the bias voltage [5].

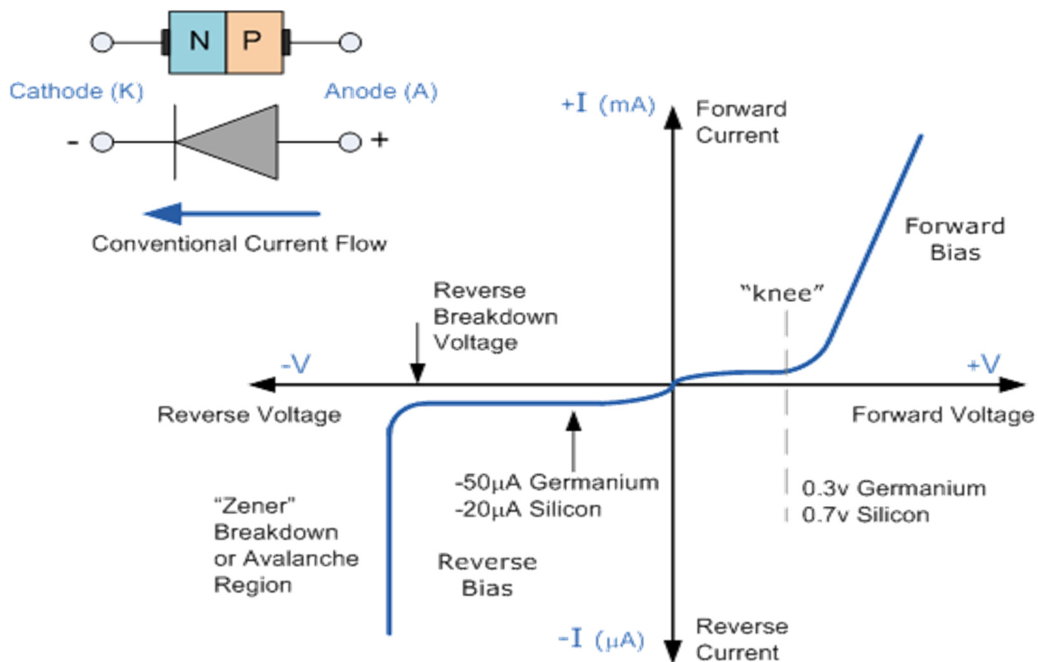

Figure 4. *I-V characteristics of a real semiconductor diode (p-n junction). Voltage axis is not to scale and breakdown can take hundreds of volts to occur.* [13]

A p-n junction's ability to block current under reverse bias has its limits. When exposed to a high enough reverse bias the junction starts to let current through. Breakdown of the junction can happen in two different methods. Either by Zener breakdown or avalanche breakdown. Zener breakdown occurs in highly doped p-n junctions in which the depletion region is narrow and has a relatively strong electric field [14]. Zener breakdown happens when an external electric field in the junction is strong enough to start tunneling charge carriers through the depletion region [15]. In contrast to the Zener breakdown, avalanche

breakdown tends to occur in junctions with low levels of doping, resulting in a wide depletion region and weak electric field. Avalanche breakdown occurs when the external electric field becomes so strong that the electrons moving through the depletion region have enough kinetic energy to create new electron-hole pairs by crashing to the lattice. This starts a multiplicative effect which results in a sudden rise in current [16]. Avalanche breakdown is often witnessed at higher voltages than Zener breakdown. It is important to note that these phenomena do not actually break the p-n junction irreversibly, as the name might imply, as long as the current moving through is kept low enough [11].

Semiconductor can also be bonded to metal forming a Schottky barrier. They are used to build mostly similar devices as p-n diodes with a non-linear I-V response. These devices, called Schottky barrier diodes, are capable of having faster response times as the operation relies on a single type of charge carrier. [5] When a Schottky barrier is formed by p-type semiconductor, the charge carrier type is holes and the forward bias is applied by applying the positive voltage to the p-side semiconductor. For an n-type semiconductor the carrier is electrons and forward bias is applied by contacting the negative voltage to the n-type semiconductor. In Schottky barrier between the metal and the semiconductor forms a depletion region acting as a barrier. Operation of the junction is similar to p-n junction, the barrier is preventing any major current flow under negative bias but breaking down when under large negative bias. The size of Schottky barrier is dependent on the semiconductor-metal combination. [5] Not every combination of metal and semiconductor form this barrier, or it is too small, resulting in an ohmic contact without rectifying properties.

2.3 Optoelectronic devices

Semiconductor devices for electrical purposes have become very popular due to multiple reasons. First of all they are relatively cheap to manufacture. Secondly they are very flexible components. Semiconductors can be manipulated and tuned through external magnetic or electric fields, adjusting the level of doping and by exposure to heat or light. Lastly, semiconductors miniaturized many existing devices and made possible a whole range of new electronic devices such as transistors.

Simple p-n junction can be used to build a myriad of devices including but not limited to different diodes, solar cells and photodetectors. Some devices consist of multiple p-n junctions such as transistors. In the scope of this thesis some important devices in terms of physical principles are inspected. Semiconductor rectifier diode and Schottky barrier diode are assessed in the previous chapter as they are closely connected to the fundamental operation of the junction.

Light-emitting diode (LED) can generate light over 15 times more efficiently than a conventional light bulb [17]. LED is essentially a p-n junction formed of direct band semiconductor. This means that minimum allowed energy of the conduction band and maximum allowed energy of the valence band are located on the same wavenumber. This results in majority of charge carrier recombination happening in a radiative manner in contrast to typical diodes where the bandgap is indirect and recombination results in heating. In a forward biased LED the charge carriers passing the depletion region can combine, which is essentially a relaxation of an excited state, leading to an emission of a photon. Energy of the emitted photons is directly the energy gap between the two states involved in the transition. Efficiency of an LED is naturally tied to probability of the recombination process in addition to the probability of the radiative recombination. Probability of recombination can be increased through introduction of Quantum Wells (QW) that trap the charge carriers in depletion region, promoting recombination. [5]

Some semiconductor devices work in a similar manner to one another but have multiple purposes. For example solar cells and photodetectors work because of the same phenomenon but are optimized for different purposes. Both devices rely on absorbing light to generate charge carriers. These charge carriers are created when a photon of a higher energy than the bandgap in the depletion region excites an electron creating an electron hole pair. Modern solar cells can do this with an efficiency over 40% [18]. Because of the built in voltage in depletion region the electron is then moved to the n-side while holes move in to the p-side. This increases the voltage over the junction resulting in a current. [19, 20] In solar cells this effect is harnessed to create energy and consequently it is desirable for the cell to absorb at a high probability in a wide range of the electromagnetic spectrum to convert light to electrical energy as effectively as possible. In photodetectors this is not as important as the desired properties are often along the lines of sensitivity, low noise, response time and linear dependence of signal compared to light intensity [21]. In contrast to photodetectors, solar cells are often build as large as possible to gather light from a large area.

Some diodes serve a unique purpose in a region where one would not at first expect, in the diode breakdown region. Zener diode is operated on reverse bias and can be used to regulate a voltage source providing stability against changes in load of a circuit. Other uses include limiting, also called clipping, which can be used to protect a circuit from high voltages or to shape the voltage signal of an alternating current source. Zener diode is often connected in parallel to the electric component to be regulated or protected. [22] If a voltage transient that exceeds the Zener breakdown voltage is experienced by the circuit, the Zener diode switches to conducting mode and protects the parallel component from the high current. The threshold for breakdown can be tailored by changing the amount of doping in the semiconductor junction sides. Higher concentrations of dopants result in lower breakdown voltages and vice versa as explained in Chapter 2.2.

Bipolar junction transistor (BJT) is the first three-terminal electrical component [5]. Transistor is a multi-junction component often consisting of three terminals. They are used in circuits to control or amplify current through two terminals by applying a current in the third terminal. Based on the operating principle transistors can be categorized in two main categories: BJTs and field-effect transistors (FET). The latter is also called unipolar transistors. In FETs the conductivity of the device is controlled by an electric field. In BJTs the operation uses both charge carriers while FETs use only a single type of a carrier. A Nobel Prize was awarded to William Bradford Shockley, John Bardeen and Walter Houser Brattain for their work in the field of semiconductors and transistors [23].

2.4 Semiconductor lasers

Laser is an acronym for “light amplification by stimulated emission of radiation”. Even though the first laser was produced in 1960, the physical possibility for such a device was recognized by Albert Einstein as early as 1917 [21, 22]. After the first practical concept, the advancements in the field of lasers became more rapid. Different kinds of lasers, such as fiber, gas, and semiconductor, were demonstrated in 1960s. The first gallium arsenide semi-conductor laser, a laser diode operating in the near-infrared, was demonstrated in 1962 by Robert Hall [1].

Laser was not an invention that was motivated by finding a solution to a certain problem. In fact, at the time of its invention, people have attributed laser as a “solution looking for a problem” [26]. Nowadays lasers have a major foothold in multiple fields with laser markets being over 12 billion dollars in size in 2017 [27]. Lasers are widely used in consumer electronics, communications, industry, medicine, research and military.

All laser operation relies on stimulated emission. Stimulated emission is a phenomenon where a photon near an atom with an excited electron stimulates the electron to transition to a lower state of energy. For the transition to occur, there has to be a possible transition for the electron that is close to the energy of the incident photon. This stimulated transition emits a photon with the same energy, phase and direction of propagation as the incident photon. Stimulated emission is demonstrated in Fig. 5. The material that stimulated emission occurs in a laser is called gain medium and lasers are often categorized by it.

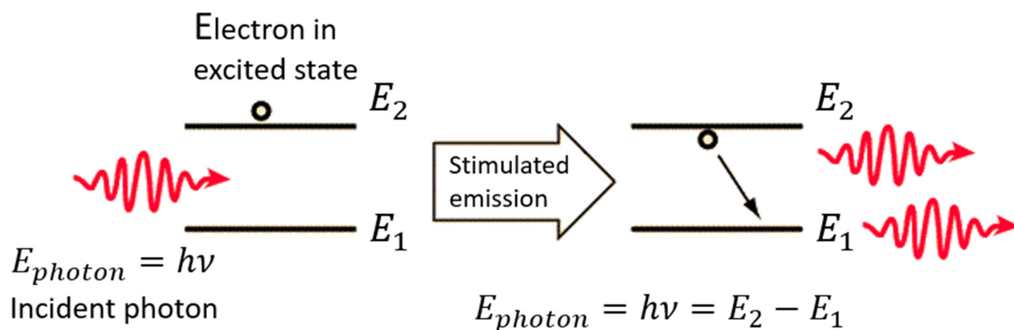

Figure 5. *In stimulated emission the energy of the incident photon has to match the energy difference between the states involved in transition.* [28]

In laser gain region sufficient ratio between the excited and non-excited particles is required for laser operation. A key threshold is the so-called population inversion which occurs when a bigger portion of the particles are in an excited state. Population inversion is also the point where the amplification for an incident flux of photons is larger than the absorption. Providing energy for the gain material, also called pumping, to achieve the population inversion is essentially the power consumption of the laser. For semiconductor lasers this is done either optically or electrically.

Laser operation also requires an optical resonator. This is because the photon flux in the gain medium, and consequently in the laser output, cannot achieve relevant powers if all the photons were to leave the laser immediately. Instead, an optical resonator surrounds the gain medium, providing a portion of the photons back to the gain medium so that further amplification can occur. Optical resonators can, for example, be comprised of naturally reflecting fiber ends, cleaved semiconductor facets or external mirrors. It is very typical for one end of the resonator to have as high reflectivity as possible and the other to have a lower reflectivity as it determines the output direction of the laser. Crude schematic of a laser is demonstrated in Fig. 6.

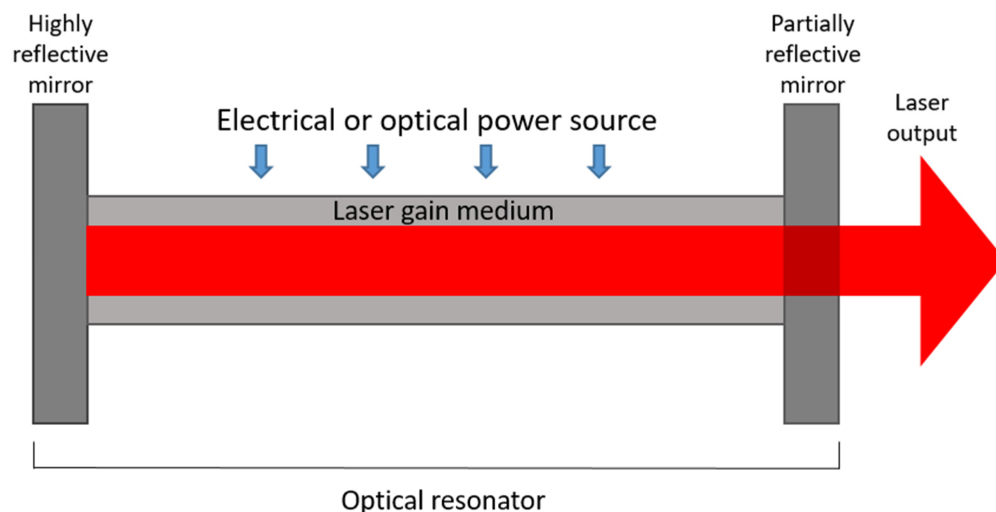

Figure 6. *Schematic of a laser with all the fundamentally essential parts: laser gain medium, power source and an optical resonator.*

Semiconductor laser uses a semiconductor heterostructure as the gain medium. By choosing the composition of the direct band gap semiconductor materials that form the heterojunctions carefully the emission wavelength can be tailored to a wide range of possibilities. Semiconductor laser structures are grown on wafers using high precision techniques that are capable of producing layers one nanometer thick such as MBE [29] and MOCVD. III-V semiconductor compositions are most commonly used, and their respective lattice constants and emission wavelengths are demonstrated in Fig. 7. An important aspect of producing laser structures with an epitaxial method is that the lattice constant of the layers have to be similar enough that the grown layer can follow the previous lattice structure. If the difference in lattice constants is too high, relaxation of the crystalline structure occurs and the properties of the structure change. The amount of strain in the layer structure can be used to affect, for example, the band structure resulting in a difference in output wavelength of the laser [30].

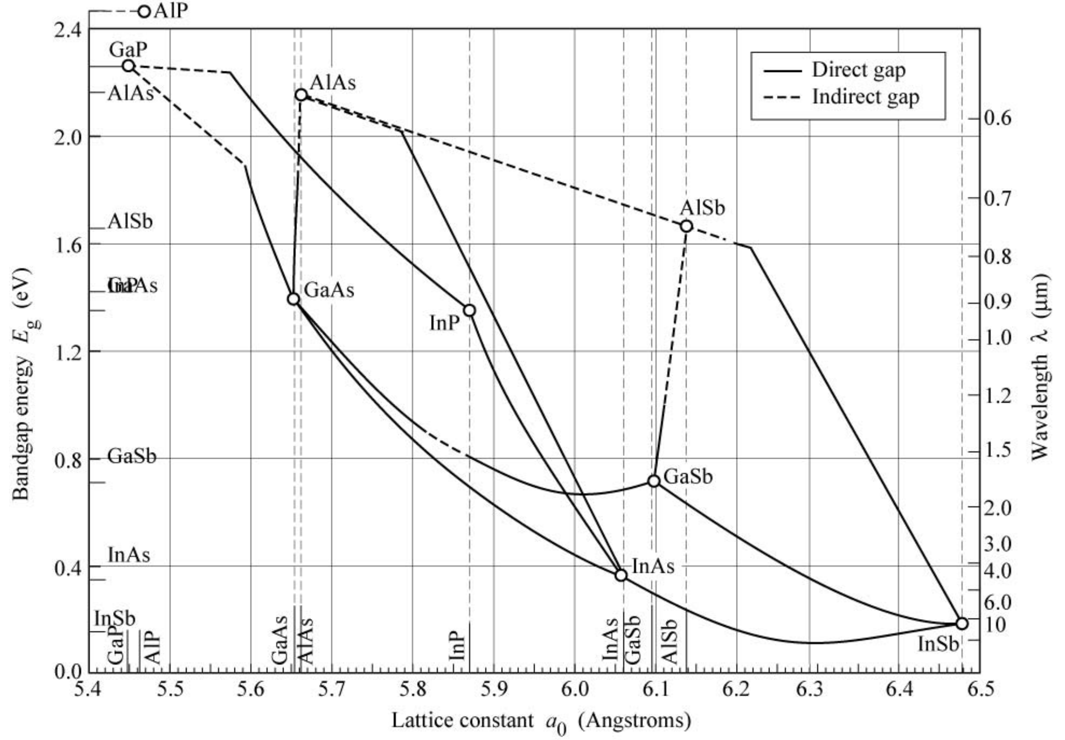

Figure 7. *Type III-V semiconductor material compositions, their emission wavelengths and lattice constants* [31].

Majority of semiconductor lasers are laser diodes [32]. Most of the laser diodes in high power applications emit light in parallel with the wafer surface and are thus called edge-emitting lasers [33]. The fundamental structure of a laser diode is a p-i-n junction, where an intrinsic semiconductor layer is located in the middle of a p-n junction [34]. The structure bears great resemblance to an LED. As light is not confined in any way in a simple p-i-n junction and population inversion is harder to achieve for a larger volume, this structure is highly inefficient.

Nowadays a structure called separate confinement heterostructure (SCH) with QWs are widely used. In SCH lasers the charge carriers and the optical field are confined separately. It uses a QW to trap the charge carriers in a very thin region making recombination efficient and layers of lower index materials to keep the light confined to a certain region. These lower index layers are also called waveguides. Threshold current density for laser operation in a quantum well laser diode

$$J_{th} = N_{QW} J_T \exp\left(\frac{\alpha_i + \left(\frac{1}{2L_c}\right) \ln\left(\frac{1}{R_1 R_2}\right)}{N_{QW} \Gamma_{QW} \gamma} \right), \tag{2}$$

where N_{QW} is number of quantum wells, J_T is the transparency current, α_i is the losses in cavity, L_c is the length of the laser cavity, R_1 and R_2 are the reflectivities of the end mirrors, Γ_{QW} is the confinement factor per quantum well and γ is the gain coefficient [35].

Vertical-cavity laser diodes are lasers which emit light perpendicular to the wafer surface. These are called vertical-cavity surface-emitting lasers (VCSEL). It uses a structure of multiple QWs and confinement layers in the middle of two distributed Bragg reflectors (DBR). The DBRs act as mirrors and provide the optical resonator in vertical direction. VCSELs have the benefit of a symmetrical beam profile in contrast to edge-emitting laser diodes. One of their main uses is as transmitters for optical fiber communications [36].

Distributed feedback (DFB) laser is a type of laser that uses a grating along the active region as an optical resonator. They are stable components and the grating is very wavelength selective [37]. This results in a narrow output spectrum. Light in the grating reflects through Bragg reflection. Output wavelength of these lasers can often be tuned by changing the temperature of the laser as it changes the period of the grating.

Vertical external-cavity surface-emitting lasers (VECSELs) are similar to VCSELs but they do not have two DBRs in the structure. Instead, the semiconductor chip is only the other end of the optical resonator, meaning the semiconductor chip has an active region on top of a DBR, and rest of the cavity is external. Dielectric mirrors are often used as external mirrors. VECSELs can reach high output powers as the mode spot size on the gain chip can be designed large and the spot can be pumped accurately using optical pumping. Excessive heating is often a limiting factor in VECSELs and diamond heatspreaders are used to conduct the heat also to the side of propagation [38]. They are also relatively modifiable as external components can be integrated to the free-space optical cavity. On the other hand, they take a lot of space and are difficult to produce reliably.

3. OPTICAL THIN FILMS

3.1 Fundamental properties

Optical thin film is a layer structure consisting of one or more layers. For the film to be considered thin, its thickness must be smaller than the coherence length of the light it is designed to interact with. Earliest days of modern thin film history dates back to Robert Boyle and Robert Hooke who noticed thin films displaying colors. Isaac Newton later associated these colors with layer thicknesses and explained the phenomenon called Newton's rings. Advances in theory of light and its wavelike nature has led to much better understanding in the field of thin films [39].

Desired characteristics for an optical thin film often include at least the following: high transparency, uniform refractive index and good physical and chemical stability [40]. Absorption of light by a thin film would not only lead to faulted performance but also rapid degradation of the film. Accurate and uniform refractive indices as well as thicknesses of the layers lead to accurate predictions on the thin film operation. Thin film structures are used mostly on the external surfaces of components and thus it is crucial that the film is as resistant as possible to deterioration by physical damage and chemical effects such as that of water vapor.

Special attention has to be paid on the compressive and tensive stresses of the materials when multiple layers are present in the thin film structure. Multiple layers with the same expressed stress can lead to the thin film adapting some other form than planar. In the case of compressive stress it leads to buckling while in the case of tensive stress the surface concaves [41]. Ideally multilayer structures are deposited with subsequent layers altering in the direction of stress as this compensates the stress resulting in high physical stability.

The underlying phenomenon behind thin films and their effect to light waves is interference. If two identical light waves that are on opposite phases interfere with each other, destructive interference occurs resulting in the light waves cancelling one another. However, if the light waves are in the same phase, amplitude of the light wave is doubled. At any given phase the amplitudes of interfering light waves can be summed to calculate the sum wave. When light hits an interface of two materials, a part of the light is reflected and the rest is transmitted. At normal incidence the reflectivity can be presented as

$$R = \left(\frac{n_1 - n_2}{n_1 + n_2}\right)^2, \tag{3}$$

where $n_1$and n_2 are the refractive indices of the materials. When light is at an interface travelling to an optically denser medium, also known as a material with higher refractive index, the part of the light that is reflected experiences a phase shift of π. Through tailoring these reflections and the phase of light through thickness of the film, transmission and reflectance can be controlled.

Light experiences distance differently depending on the refractive index of the medium that light is propagating in. This has to be accounted for when calculating the phase of the light wave after a certain distance of propagation. Thickness of a thin film as light experiences it is called optical thickness. It is the physical thickness times the refractive index of the film. One has also to be mindful of that refractive index is dependent on the wavelength of the light. This phenomenon is called dispersion.

3.2 Anti-reflective coatings

Anti-reflective (AR) coatings are used to reduce the reflection from a surface. In many applications, including eye glasses, they are used to reduce the reflection of an air-glass interface. Even though the reflection of an air-glass interface is only a few percent in size, it is still noticeable by human eye and causes complex multi-lens systems to be futile without proper AR coatings. As shown in Eq. 3 the surface reflection gets larger as the difference between refractive indices of materials increases. This makes AR coatings an important part of semiconductor surfaces which typically have high refractive indices.

The simplest AR coating is a single layer. The layer must be a quarter of the wavelength in optical thickness. This causes the waves reflecting from the interfaces to have exactly opposite phases and thus interfering with one another destructively. For optimal performance the reflected waves should be equal in amplitude. This can be achieved, as shown by Eq. 3, with a film with a refractive index of

$$n_f = \sqrt{n_1 n_2}, \tag{4}$$

where $n_1$and n_2 are the refractive indices of the propagation media. This results in virtually perfect transmission for a single wavelength. This is a serious limitation for single layer AR coatings as refractive index of a material is not a parameter that can be altered freely.

AR coating can also consist of two or more layers. These designs are used when wider wavelength range of high transmission is required or some special behavior is required on multiple different wavelengths. Multilayer AR coatings are not so heavily limited by the refractive indices of the coating materials in contrast to single layer AR coatings that can only result in very high transmissions when the refractive index of the thin film is in a very narrow range depending on the substrate. For example, single layer AR is not an efficient solution for glass substrate with a refractive index of 1.52. This is because the

lowest refractive index material suitable for thin films has a refractive index of 1.38 while the optimal refractive index according to Eq. 4 would be 1.23, given that the incident medium is air. [39] Multilayer AR coatings are much more complicating to calculate and underlying method of operation can change from quarter wave thick layers to layers with some other thickness [42]. Computer programs are widely used to refine these coatings but often require a well-chosen initial structure to find a good solution [41]. Demonstration of different AR coatings is shown in Fig. 8.

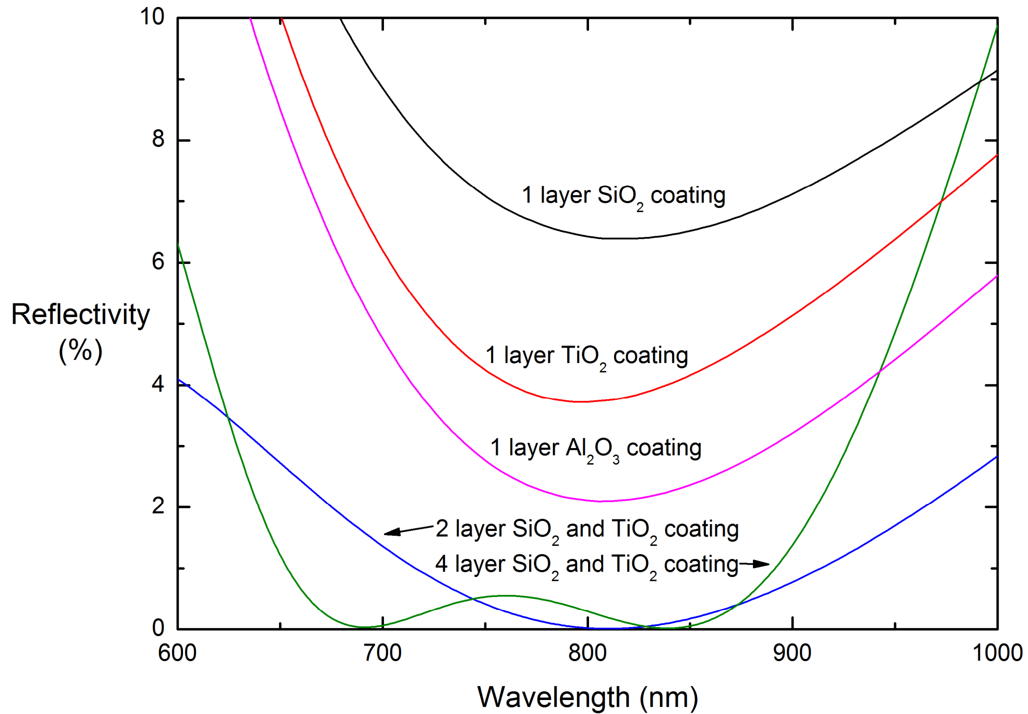

Figure 8. *Different AR coatings on air-silicon interface. Refractive indices at 800 nm wavelength for SiO_2, TiO_2, Al_2O_3 and Si are 1.48, 2.34, 1.66 and 3.69 respectively. Single layer AR coatings of these materials cannot be used to achieve low reflectivity. According to Eq. 4 the zero reflectivity AR coating could be achieved with refractive index of roughly 1.92 and since the refractive index of Al_2O_3 is nearest to this, it forms the best single layer AR. Two-layer AR can be used to achieve virtually zero reflectivity. Note how four-layer AR does not improve the target specific transmission but can be used to widen the width of low reflectivity region significantly.*

3.3 High reflective coatings

History of high reflective (HR) coatings date back to the ancient times where polished metal surfaces were used as mirrors [43]. Even in the present these general mirrors have their purpose, only the production method is different. Metal mirrors are produced nowadays by evaporating a metal thin film to a substrate. For example, both silver and gold reflect infrared (IR) light near perfectly. Reflectivity of aluminium, silver and gold can be seen in Fig. 9.

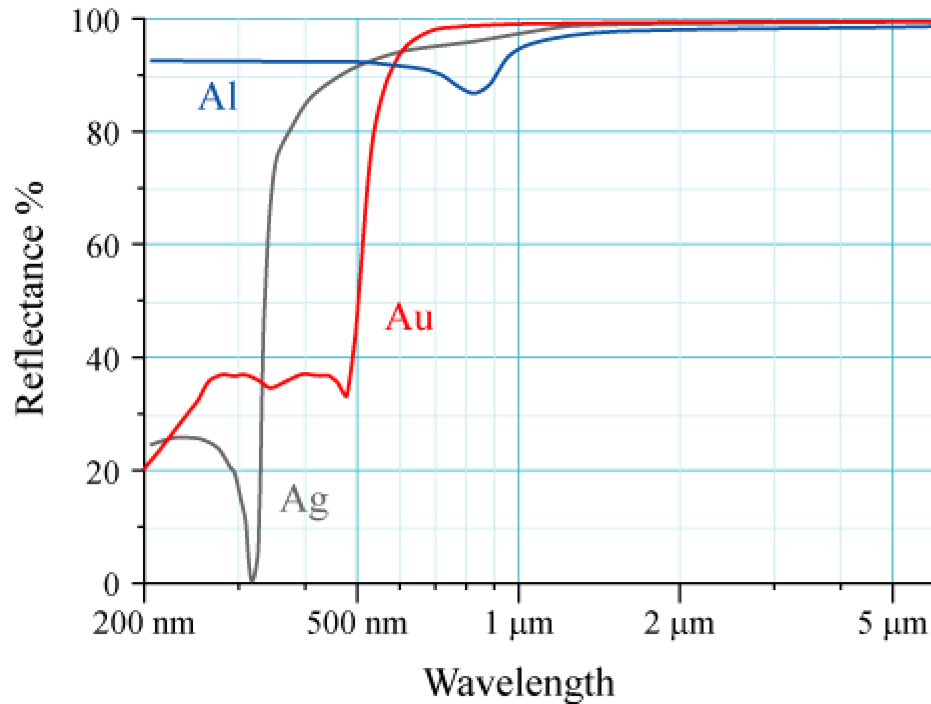

Figure 9. *Reflectivity of aluminium (Al), silver (Ag) and gold (Au).* [44]

Metal mirrors come with a few inherent flaws making them unsuitable for a variety of applications. Almost all metal mirrors, excluding gold, oxidise easily altering their reflective properties. This makes them unsuitable for precise applications at least without a protective coating. As metal mirrors are filled with free electrons, they absorb much of the light that they do not reflect. Usage of a metal mirror as an end mirror of a laser would quickly lead to a destruction of the mirror as the absorption results in heat production [41].

Dielectric materials are once again a good solution to provide high reflectivity with very little absorption. Even though the reflection at a single interface is not large due to limited refractive index of the materials, with the use of a periodical structure and constructive interference very high reflectivities can be achieved. These distributed Bragg reflectors (DBR) consist of quarter wave thick low and high index pairs. Every added pair of layers enhance the reflectivity but is essentially limited by physical stability of the layer structure. Naturally the reflection is also higher the more material pairs refractive index forming the DBR differs from one another.

DBRs produce the highest reflectivity when the stack is started and finished with the material that has the highest contrast in refractive index compared to adjacent media. For a structure of an even number of pairs, such as DBR structure between semiconductor and air, low index layer is facing the semiconductor while high index layer is facing air at the end of the stack.

The reflectance of a DBR can be derived from matrix formalism. Matrix formalism is a way to treat individual layers and their surfaces in a thin film system as matrices whose effect to the wave function of incident light can be calculated by solving the product of the matrices. The wave function at the outer surface can be written as a product of the transfer matrix M and the wave function at the substrate surface:

$$\begin{bmatrix} A_0 \\ B_0 \end{bmatrix} = \begin{bmatrix} M_{11} & M_{12} \\ M_{21} & M_{22} \end{bmatrix} \begin{bmatrix} A_s \\ B_s \end{bmatrix}. \tag{5}$$

Effect of interfaces and the propagation media itself to the wave function can be written by different matrices. Propagation inside an individual layer is represented by a propagation matrix

$$P_l = \begin{bmatrix} e^{i\Phi_l} & 0 \\ 0 & e^{-i\Phi_l} \end{bmatrix}, \tag{6}$$

where i is an imaginary unit and Φ_l is the phase shift. It can be given as

$$\Phi_l = \frac{2\pi n_l(\lambda)}{\lambda} d_l \cos(\theta_l), \tag{7}$$

where λ is the wavelength of the light, $n_l(\lambda)$ is the wavelength dependent refractive index of the layer, d_l is the physical thickness of the layer and θ_l is the angle of incidence for the light. Light waves behave differently at the interfaces depending on their polarization. If the electric field is parallel to the plane of incidence, the plane which is formed by the light before and after interacting with the interface, the polarization is called transverse magnetic (TM) polarization. Similarly, if the electric field is perpendicular to the plane of incidence, the polarization is called transverse electric (TE) polarization. [41] TM polarization is also called p-polarization while TE polarization is also called s-polarization. Behaviour at the interface can be given by following matrices for p-polarization

$$D_{l,p-p} = \begin{bmatrix} \cos(\theta_l) & \cos(\theta_l) \\ n_l & -n_l \end{bmatrix} \tag{8}$$

and for s-polarization

$$D_{l,s-s} = \begin{bmatrix} 1 & 1 \\ n_l \cos(\theta_l) & -n_l \cos(\theta_l) \end{bmatrix}. \tag{9}$$

Using the propagation and interface matrices the transfer matrix M can be written for an arbitrary number of layers, including the outer medium and substrate, as following

$$M = D_{l,o}^{-1}\left(\prod_{l=1}^{N} D_l P_l D_l^{-1}\right) D_{l,s}, \tag{10}$$

where $D_{l,o}$ and $D_{l,s}$ is the interface matrix for outer medium and substrate respectively. It is important to note that simply the layer matrix is used when entering the layer opposite to when exiting the layer. For exiting the layer, the inverse of layer matrix is used.

Now let's consider a DBR on top of a semiconductor laser diode facet. In this case the interface that the DBR is on is air-semiconductor. The DBR is deposited so that first layer grown on the semiconductor is a layer of low refractive index and the stack ends in a layer of high refractive index. Incident angle in the case for edge-emitting laser diode can be considered perpendicular and we can assume dispersion to be insignificant. DBR layers are quarter wavelength of optical thickness, thus the physical thickness of DBR layers for wavelength λ can be written as

$$d_l = \frac{\lambda}{4n_l}. \tag{11}$$

By inserting this to the Eq. 7 and further calculating the propagation matrix for DBR from Eq. 6, we get

$$P_{DBR} = \begin{bmatrix} i & 0 \\ 0 & -i \end{bmatrix}. \tag{12}$$

As we considered the incident angle θ_l to be 90°, the interface matrices $D_{l,p-p}$ and $D_{l,s}$ simplify to form

$$D_l = \begin{bmatrix} 1 & 1 \\ n_l & -n_l \end{bmatrix}. \tag{13}$$

As the DBR for air-semiconductor interface is formed of N amount of low and high index pairs and according to Eq. 10, we can write the layer matrix as

$$M = D_{l,o}^{-1}\left(D_{l,H} P_{DBR} D_{l,H}^{-1} D_{l,L} P_{DBR} D_{l,L}^{-1}\right)^N D_{l,s}, \tag{14}$$

where $D_{l,o}$, $D_{l,H}$, $D_{l,L}$ and $D_{l,s}$ are interface matrices for outer surface, high index layer, low index layer and substrate media respectively. These can be formed by inserting the layers corresponding refractive index to Eq. 13. After some inverting and multiplication of matrices we end up with a result

$$M = \frac{(-1)^N}{2} \begin{bmatrix} \left(\frac{n_L}{n_H}\right)^N + \frac{n_s}{n_o}\left(\frac{n_H}{n_L}\right)^N & \left(\frac{n_L}{n_H}\right)^N - \frac{n_s}{n_o}\left(\frac{n_H}{n_L}\right)^N \\ \left(\frac{n_L}{n_H}\right)^N - \frac{n_s}{n_o}\left(\frac{n_H}{n_L}\right)^N & \left(\frac{n_L}{n_H}\right)^N + \frac{n_s}{n_o}\left(\frac{n_H}{n_L}\right)^N \end{bmatrix}, \tag{15}$$

where n_L, n_H, n_o and n_s are the refractive indices of the low index film, high index film, outer medium and substrate respectively.

Reflectivity of the DBR structure can be calculated using the components of transfer matrix M as following

$$R = \left|\frac{M_{21}}{M_{11}}\right|^2. \tag{16}$$

After some relatively straightforward mathematical operating we obtain a result

$$R = \left|\frac{\frac{n_s}{n_o}\left(\frac{n_H}{n_L}\right)^{(2N)} - 1}{\frac{n_s}{n_o}\left(\frac{n_H}{n_L}\right)^{(2N)} + 1}\right|^2, \tag{17}$$

which can be used to calculate the maximum reflectivity of a DBR stack consisting of N pairs of low index and high index pairs for layer materials, substrate and outer medium of arbitrary refractive indices. Reflectance of TiO_2 and SiO_2 DBR stack with an even number of pairs and silicon as substrate is shown in Fig. 10. The more layers are in the DBR structure, the sharper featured the shape becomes. Periodic sidebands are also typical for DBRs.

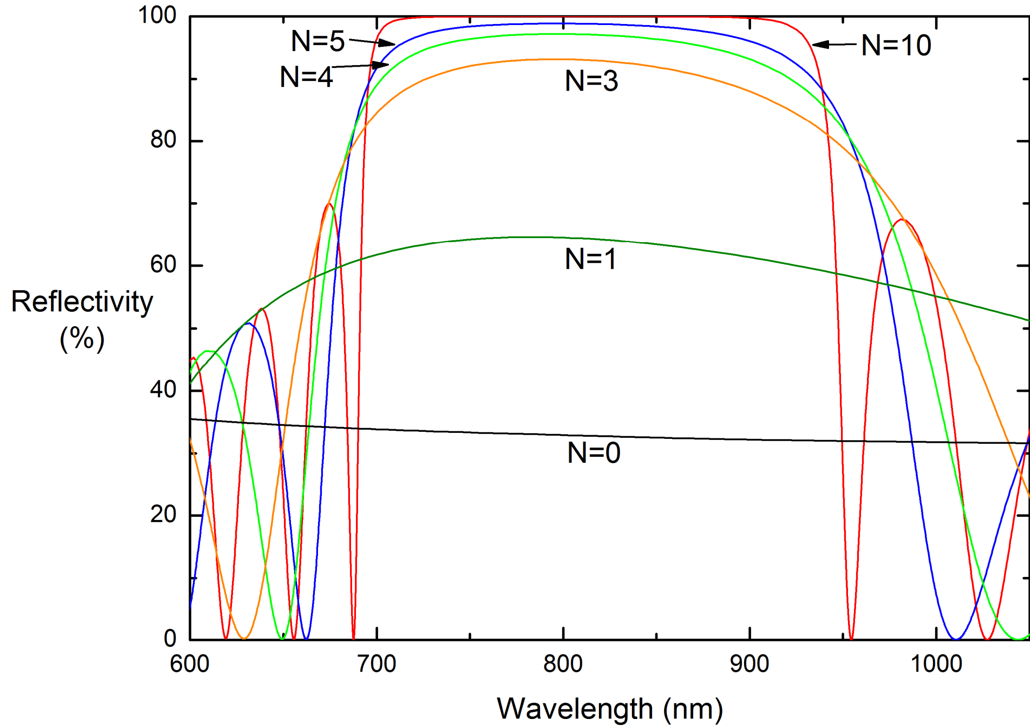

Figure 10. *Reflectivity of a DBR structure formed of 85.6 nm thick TiO_2 and 134.9 nm thick SiO_2 on silicon with 1, 3, 4, 5 and 10 pairs for wavelength of 800 nm. Refractive indices for TiO_2, SiO_2 and silicon are 2.34, 1.48 and 3.69 respectively. Plain air-semiconductor interface is noted as N=0 in the figure.*

Dielectric mirrors, when compared to metallic mirrors, have only a small region of high reflectivity. Width of the high reflecting region can be increased through increasing the number of layer pairs or by selecting larger contrast material. However, this leads to lower reflectance in specific wavelengths, in contrast to traditional DBR, and physical instability due to thickness of the structure. The size of the high reflecting region of a traditional DBR from the centre wavelength λ_0 to edge of the region λ can denoted as

$$\Delta g = \frac{2}{\pi} \arcsin\left(\frac{n_H - n_L}{n_H + n_L}\right), \tag{18}$$

where

$$g = \frac{\lambda_0}{\lambda}. \tag{19}$$

As can be seen the width of the high reflection region is a function of only the refractive indices of the layer materials [39]. When the difference between refractive indices increases the region widens.

Some applications require even more specialized filters such as edge or notch filters. Edge filters are designed to reflect or transmit light of shorter wavelength and do the opposite for longer wavelength. In case the shorter wavelength is blocked, the filter is called a long

pass filter and in case of the opposite the filter is called short pass filter. Notch filters are designed to attenuate a certain wavelength range while letting through the others. Its counterpart, band-pass filter, does the opposite transmitting only a certain wavelength range.

3.4 Adhesion and abrasion

Optical thin film structures are prone to physical and environmental threats. Even something as little as a light touch of a finger on surface of the film can lead to impaired performance as contaminants attach to the surface. Under normal operating conditions the failure of a coating can be attributed to the film detaching from the surface or abrasion such as scratching on the coating. Most common environmental threat is arguably humidity which tends to soften up the coating making it more sensitive to abrasion.

Testing different aspects of mechanical stability of a thin film is not always simple. Administering a physical force that stays the same across measurements is challenging. The measurements are also of such nature that they can often only be applied once. Absolute limits of mechanical stability and hardness are not often sought for, but the coatings are tested against a set of predetermined requirements in a pass or fail manner.

Adhesion between the film and substrate can be measured by so called tape test. By knowing the peel adhesion rating of the tape, one can test if the adhesion of the film is greater of lower than the one of the tape. It is crucial to the consistency of the experiment that the tape is pulled off the surface smoothly and always at the same angle. Thickness of the tape should not be changed as increase in thickness results in a slightly less harsh interaction with the film [39]. Popular tape for adhesion tests is 3M 650 Scotch Cellophane tape that is for example used in an American military standard MIL-F-48616 [45]. Extra attention should be paid to the cleanliness of the coated surfaces as contamination can result in a drastic reduction in adhesion. This can also be caused by crystalline defects in the substrate.

Abrasion resistance of the film can be tested using a test instrument that applies a constant force to the surface. Depending on the severity of the test either specific cloth or rubber eraser is used. The test instrument is dragged multiple times over the film with a constant force applied. The instrument should be held as upright as possible and moved with a constant speed. After the abrasion the film is cleaned and the scratches caused to the film are to be counted and measured. Once again, this measurement does not exactly quantize the robustness of the film but gives an understanding of how much abrasion the coating can handle before it is considered unusable. It is also important to note that the observed hardness of the film is not only to be a function of the material and evaporation parameters but thickness of the film [39].

Depending on the application the coating may be exposed to certain environmental threats such as humidity, vibration and rapid temperature variations or extremities. Effects of environmental harm caused to the thin film range from failure of adhesion to corroding or dissolving the film. A rather universal test, also in accord with MIL-F-48616, is to expose the film to a high humidity and a temperature of 50 °C for 24 hours and perform a standard abrasion test within an hour [35,42].

4. ION BEAM SPUTTERING

4.1 Basic properties

Ion beam sputtering (IBS) is a method of depositing thin films by bombarding a target material with an ion beam. If these ions have enough energy, they can dislodge atoms from the target material. This is called sputtering. The ejected particles then propagate away from the target resulting in a controlled method of thin film deposition. A high-end IBS machine consists of vacuum pump, material targets, two ion sources, optical monitoring system and various gas lines. Second ion source is not required but its absence limits possibilities of deposition methods. Picture of IBS chamber is shown in Fig. 11.

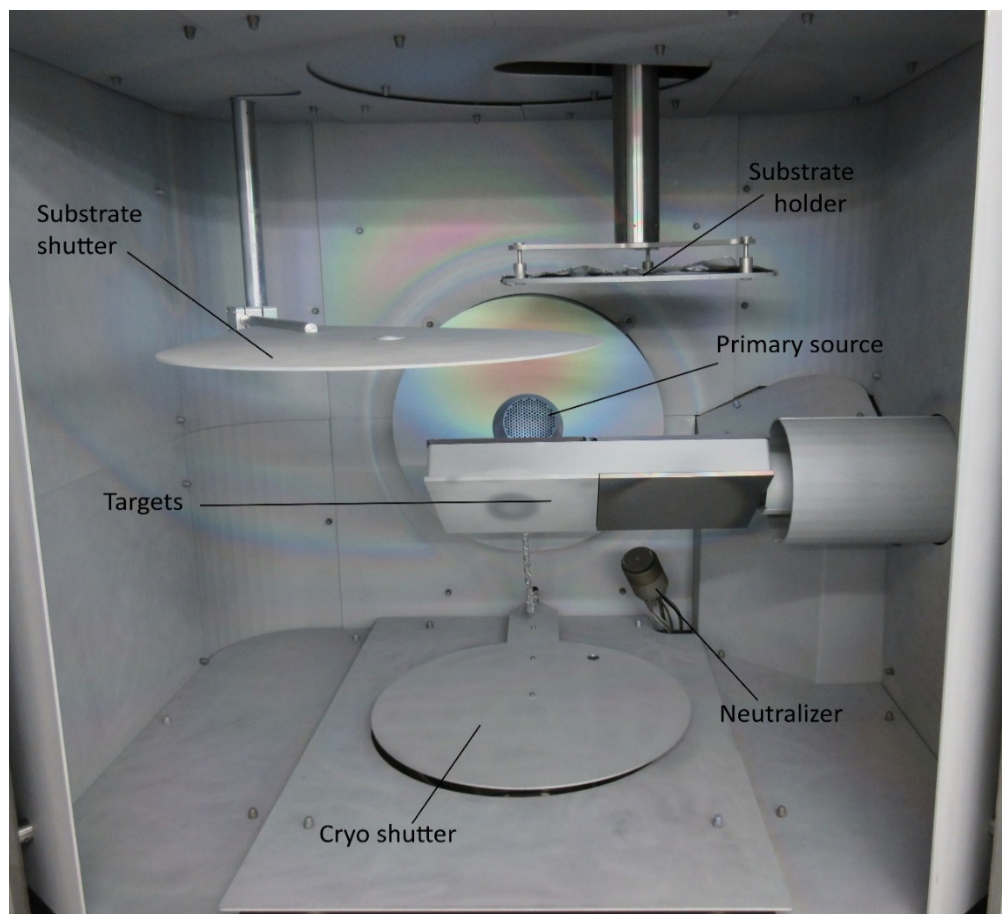

Figure 11. *Coating chamber of the IBS made by Cutting Edge Coatings used in this thesis. Optical monitoring beam as well as cryo pump are located under the cryo shutter and the optical detector is located above the chamber roof.*

The clear majority of modern optical coatings are produced in a vacuum. More specifically, around one millionth of atmospheric pressure. Vacuum conditions contribute to the controllability of the process mainly by two methods. Firstly, it increases the mean free

path of the particles which allows more particles to reach their desired location preferably without losing energy along the way in collisions [46]. Secondly, low pressure allows the maintaining of a controlled gas combination in the chamber which is required to deposit certain films with high reproducibility. Cryo pumps are often used because of their quick pump times. Industrial machines are often equipped with a load lock chamber to prevent the venting and pumping of the whole chamber.

Ion source is a device that generates ions and accelerates them. In the case of the primary source the ions are directed towards the material targets to sputter while in the assist source the ions are sent straight to the device to be coated. The assist source can be used for example to clean the device prior to coating or to alter the properties of deposited material through introducing energetic ions to deposition surface. The latter is called ion assisted deposition (IAD).

In practice, ion source requires four components to operate: a chamber for plasma generation, a method to bring in material for ion generation, power to ionize the material and an electric field to accelerate the generated ions out of the source [47]. Kaufman ion sources are often utilized in tasks that require a high current density ion flow with a low individual ion energy as their multi-aperture ion optics are able to meet these requirements [46, 47].

Gridded radio frequency (RF) ion sources generate plasma using a coil encircling the plasma generation chamber. The rapid alternating current generates sudden and strong changes in the magnetic field, inductively generating the plasma. [50] At the output of the ion source are three grids with tunable voltages. The ions move to the accelerating grid due to pressure difference and are shot out of the ion gun by the electric field between the grids. By alternating the power input of the coil, the voltages of the grids as well as the flow of input gas, the ion beam shape, current density and ion energy can be controlled. Schematic of an ion gun and its electrical configuration is shown in Fig. 12.

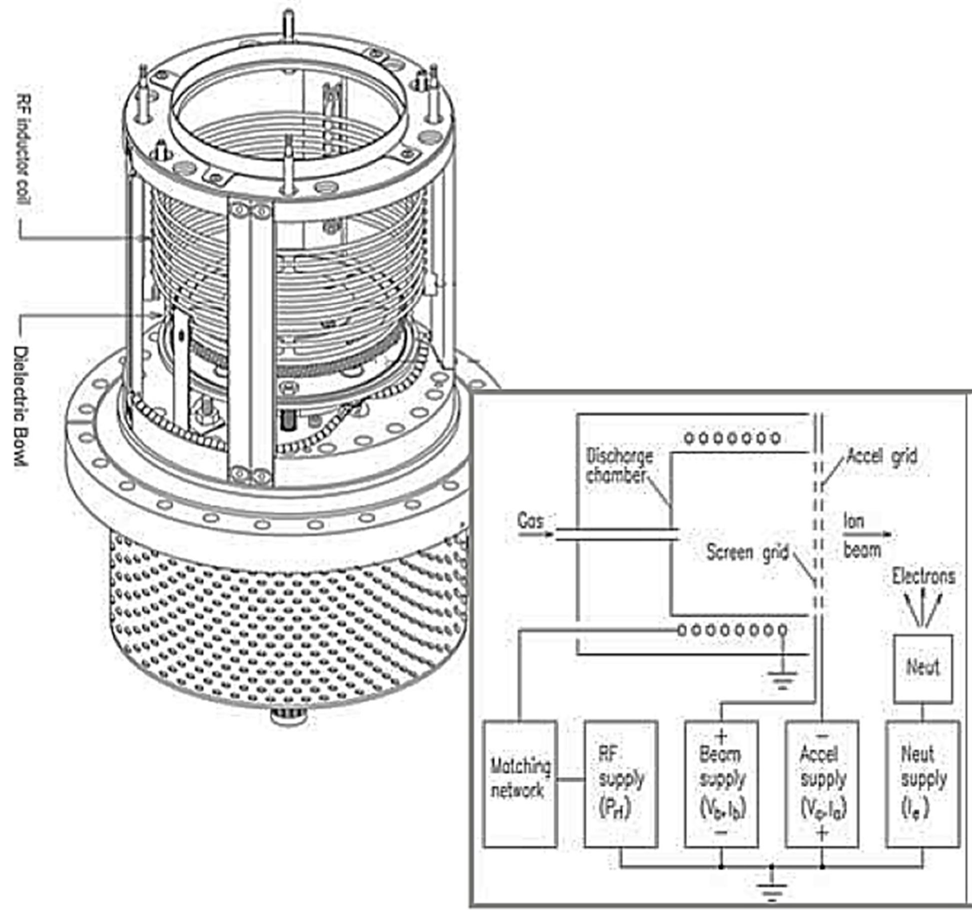

Figure 12. *Schematic of a gridded radio frequency ion source and its electrical configuration. Grids are not in the model picture and would be inserted on top of the ion source* [51].

After accelerated ions leave the ion source, they are neutralized. This is done by a neutralizer which is essentially an electron source. Neutralizing the ion beam protects any electrically sensitive components during the coating and is required when depositing dielectric materials because of harmful surface charging effects [52].

Similar radio frequency technology can be used to produce an electron source as well as an electron gun. The key difference is that in a neutralizer the ions are collected inside the discharge chamber while the electrons are attracted to the output. The number of electrons produced in certain amount of time is proportional to the power of the coil. Graphic illustration of a neutralizer can be seen in Fig. 13.

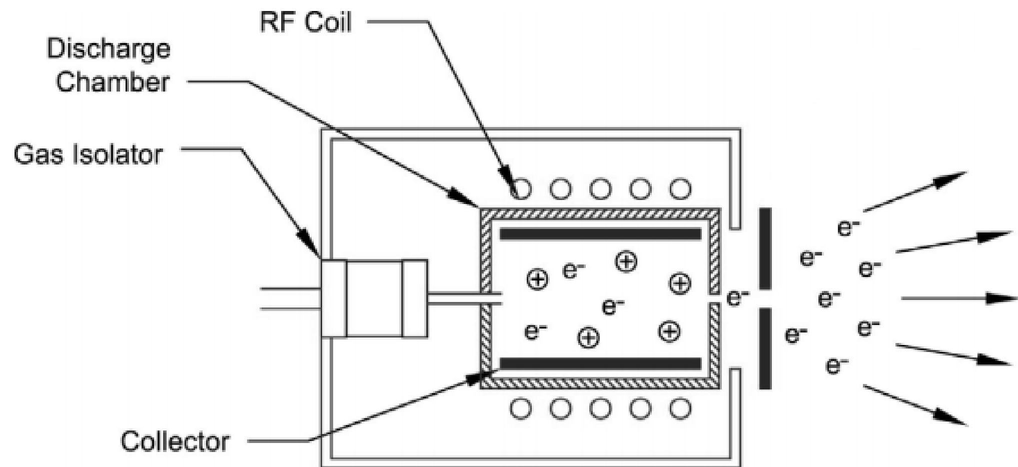

Figure 13. *Cross section illustration of a radio frequency electron source. It provides electrons to neutralize the ion beams from the ion sources.*

Sputtering gases are brought to the ion sources and neutralizer individually through flow controllable gas lines. Primary ion source uses noble gases such as argon that do not react with the target material if the desired coating consists of only the target material. It is also possible to grow silica films, for example, by using a silicon target and sputtering it with oxygen ions. It is also possible to influence the characteristics of the deposited material by introducing a background gas to the deposition chamber. In contrast to the primary source, the assist source can be used for variety of purposes such as cleaning. This results in a benefit for linking multiple gases to the assist source.

The targets that the primary source ion beam is launched at are attached to a movable holder. The number of targets vary depending on the intended use of the machine. The targets should be large enough that most of the ions from the ion source hit only the desired target. Even though sputtering the adjacent material limits the usable area on the target, having two or more targets next to one another has its merits. For example, two targets next to each other facilitate the deposition of graded index films which can be utilized in special applications [53].

Samples are inserted to a rotating substrate or sample holder. Height of the holder is an important parameter regarding the deposition speed and uniformity and thus should be adjustable through the operating software. The holder also rotates to achieve better film uniformity as well as permitting optical monitoring of the deposition.

Material targets erode under the effects of a high energy ion beam, as the premise of sputtering suggests. The region of the material target that is exposed to the center of the ion beam wears off the quickest. Also, the surface of the targets exposed to the ion beam tends to roughen, forming somewhat irregular surface. These cause the deposition rate to vary over the lifetime of the material target. This change as well as other changes can be

accounted for by calibrating the materials before deposition. The need for calibration can be avoided by implementing a monitoring method such as an acoustical resonator or an optical monitoring system to observe the deposition of a film in real time.

Optical monitoring systems operate by comparing a signal beam that has passed through a glass monitoring piece to a light beam that has not been altered. This can be achieved by rotating the sample holder, which has two holes in it. In other one of the holes is a glass monitoring piece and the other is left empty as a reference. The detector then analyses the wavelength dependent transmission levels to calculate the amount of material deposited on the monitoring glass piece. Refractive indices of the deposited materials are given as a function of wavelength to the system beforehand.

4.2 Facet cleaning

Semiconductors are prone to surface oxidation when exposed to ambient air. These native oxides affect the performance of a semiconductor laser negatively. Semiconductor materials containing aluminum can form an oxide layer 5 Å thick as fast as in 10 min [54]. It is important to note that the oxidation time of edge-emitting laser starts only when they are cleaved from the wafer. The optical resonator is not in contact with external gases until a part of the wafer, which from the laser components are made from, is cleaved to smaller pieces which exposes the laser facets. However, the initial oxidation process of a semiconductor surface is almost instantaneous and the whole cycle of producing semiconductor lasers should be performed in a vacuum if oxidation were to be avoided. This is highly impractical as it would require performing of multiple high precision process steps without exposing the devices to room air.

The oxide compounds formed on semiconductor surfaces can be cleaned in an IBS using the assist ion source. The oxides, as well as any other contamination, are harmful as they increase the density of surface states on the semiconductor surface resulting in increased absorption and heating [55]. The principle operation of cleaning is essentially sputtering; ions are fired from the assist source until the oxide layer is removed. One advantage for this type of cleaning treatment is that as a certain thickness of surface material is physically removed, organic contamination and some smaller particles like dust are also removed in the process. As the cleaning is done in a vacuum, adsorbed gases are also removed [2].

The ions that are used for facet cleaning should be of much lower energy than the ions used for target sputtering. Higher ion energies than 550 eV are generally avoided [56] as they can cause damage to the semiconductor structure by breaking bonds or implementing into the crystalline structure. Too high ion energies can also cause surface contaminants to penetrate the crystalline structure or cause mixing of layers in the semiconductor.

Lower boundary of ion energy is limited either by the operating parameters of the ion source or a too low current density bombardment ions [52].

Energy of an individual ion and current density of the ion beam can be altered by tuning the operating parameters of the assist ion source. Voltages between the accelerating grids affect directly to the energy that the ion is accelerated to. Power at the coil that generates the ions as well as the gas flow to the ion generating chamber determines the number of ions leaving the chamber. Grid voltages also affect the shape of the ion beam. Shape of the beam and the number of ions generated ultimately determine the current density of the ion beam. To achieve a smooth cleaning of the facet preferably high current density, meaning high amounts of ions per second, of low individual energy are used.

The chemical composition of ion beam can be changed by introducing a different gas combination to the assist ion source. Heavier and inert gases such as argon clean the facet mostly physically while lighter and more reactive gases like nitrogen and hydrogen have also a chemical effect. Effects of the reactive gases depend on the material they react with. For example, forming different hydrides and nitrides to the surface. Reactions vary also as a function of ion energy as a low energy particles react less with the material.

Exposure time is an important variable of the cleaning process. Because thickness of the oxide layer varies as a function of oxidation time and the composition of the semiconductor structure, cleaning treatment duration can be hard to optimize. Ideally the so-called "cleave to coat -time" of semiconductor lasers should be constant with variation only in the order of minutes. Then the treatment time can be matched with each used semiconductor composition. The fact that the native oxides formed by semiconductors tend to be harder than the semiconductor itself increase the importance of time as excessive etching of the semiconductor does not benefit the device.

For facet cleaning to influence the surface, reoxidation should be avoided. Evidently, the cleaned surface should not be exposed to ambient air before the coating process is complete or the oxidation will repeat. However, oxides are widely used as materials for thin film coatings for semiconductors. This means that during coating oxygen is present in the coating chamber. Depending on the method, reoxidation during coating can occur because of the small background pressure of oxygen in the chamber or if oxygen is used as operating gas for the primary ion source.

It is possible to avoid reoxidation of the surface by depositing a very thin passivation layer. The layer should be thin enough to not influence the interface optically but thick enough to prevent oxygen from passing through. Silane and silicon nitride are widely used passivation layers with semiconductor devices such as transistors and solar cells [56–58]. Some degree of passivation can also be achieved by using gases such as nitrogen and hydrogen in the cleaning treatment because they react with the surface to form compounds that cannot be oxidized.

4.3 Catastrophic optical damage

Catastrophic optical damage (COD) or catastrophic optical mirror damage (COMD) is an irreversible damage caused by higher power density than the laser structure or facets can withstand. COD is an abrupt phenomenon that renders the laser device unusable. COD can occur inside the semiconductor structure or in the laser facets. However, the AR facet is much more susceptible to COD [60] as this is where the laser output is and thus transmits higher powers than the HR facet.

COD occurs because of some impurity or defect that absorbs light and generates heat in the structure. This means that somewhere in the structure there is an energy state with small enough bandgap to absorb light. As the defect or impurity absorbs light, it heats up further reducing the bandgap energy and causing the material to absorb even more light. Thus the process is accelerated by a positive feedback loop that ends to temperature rising over some critical point and occurrence of COD. [61]

COD threshold and the effect of coating to it is best tested under pulsed laser operation. This is because short optical pulses with a low duty cycle minimize the heating of the laser component, giving it time to cool down between optical pulses. COD occurs at lower optical power if the laser is operated at a high temperature. Usage of short enough current pulses for the laser diode greatly reduces the variation in thermal conductivity of individual devices stemming from the process of attaching semiconductor laser chips to submounts. Pulse length of 2 μs has been reported for diode laser COD testing [60]. Shorter pulses can also be used but pulse sources that generate very short pulses cannot generally reach high currents and vice versa.

Prior to COD testing the devices must be mounted to a submount. The submount contains at least 2 pads from which the other is connected to the positive pins and the other to negative pins. The submount pads are connected to one another by bonding wires from on top of the laser device to the other pad closing the electric circuit. The mounting and input of current must be done so that the device is positively biased. Thermally and electrically conductive glue is used to hold the laser chip tightly in place. Laser chips are generally mounted p-side, the side of active layers, against the submount. This is because the semiconductor substrate, n-side, is not a good heat conductor and most of the heat is generated at the p-side. However, COD tests can be done with p-side up mounted devices assuming that the pulse length is short enough and the duty cycle small enough, giving the device time to release the heat between pulses.

Ideally COD test is performed in a single measurement as the devices wear out during operation [62]. It is also highly important that the ramping up of current is done similarly as with the other devices. This can be done by operating the pulse source from a computer. Consistent step size when increasing current and stabilization time, the time how long one measurement point is measured for, can be given to the program.

Measurement of laser power during testing can be approached in multiple ways. One option is to use standard power meter, preferably integrating sphere for high accuracy. As the power shown by the power meter is the average power at the power head, the peak power of pulses can be calculated when the duty cycle is known. Peak power measured this way is prone to error as the optical pulse is never a true tophat pulse due to limited speed of the components, effects of impedance in the conducting wires and rise times of the current pulse source. Other method involves a high speed photodetector. This way the power can be measured from the pulse when the power is at its highest. Measuring spectral data in tandem with the power is beneficial as heating of the component can be approximated from the changes in laser emission wavelength.

CODs that occur on the AR facets are visible with a microscope. The damage can vary from a miniscule black dot to a black burnt line as wide as the emitter itself with craterlike damage embedded in the line. As mentioned before, the AR facet is must susceptible to COD and thus the damage can often be analyzed visually. AR facet should be examined before testing of the device as well in case the chip has somehow damaged or contaminated during the mounting process. The same examination can also be done on the p-side, if the devices are mounted p-side up, to make sure that the laser chip has not damaged during the mounting. This way CODs that occurred for other reasons can be screened out of results as the device failure did not occur because of the optical coating or the semiconductor structure. Demonstration of a line type COD is shown in Fig. 14.

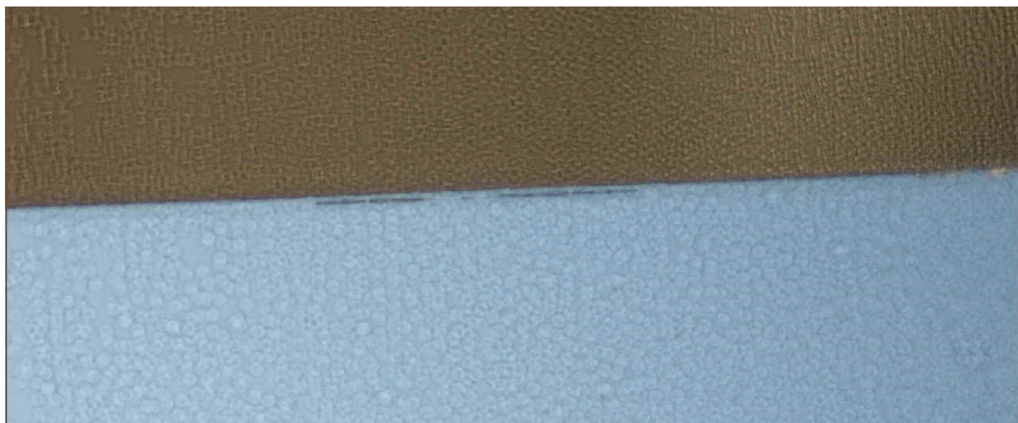

Figure 14. *Typical COD on a semiconductor laser facet. The laser facet is blue and the brown area is background. The COD is the black lines and dots near the upper edge of facet.*

4.4 Semiconductor laser diode life time

The failure modes of semiconductor laser diodes are summarized in three different categories according to S. L. Yallen et. al. in publication "*Reliability of GaAs-Based Semiconductor Diode Lasers: 0.6-1.1 µm*" [63]. At operating powers of 50 to 100 % of average COD threshold the laser degradation is mainly due to optical power density at the facets. The amount of optical power density at the laser facets correlates with the speed of degradation. At regions of low optical power, the main degradation shifts point defect generation, which is believed to be caused by current. The third failure mechanism is independent of optical power and is caused by changes in the active region of the laser, often witnessed as dark line defects.

Continuous operation at high optical power densities causes facet degradation. One contributor in this degradation is the diffusion of oxygen from the facet coatings. Rate of facet degradation is also increased by presence of moisture [64]. This happens unusually fast in semiconductor compositions containing aluminum, which oxidizes easily. [62] This kind of facet degradation is usually associated with COD as the main failure method. Diffusion at the laser facets increases absorption eventually lowering the threshold for COD until it occurs.

Point defects in the semiconductor structure are essentially dislocations in the crystal lattice. As well as reports of generation of point defects because of operating current [63], they are also generated by mechanical stress and reside in the lattice even before operation due to growth errors in the lattice. If the point defect spreads along the crystal plane, it can be called a dark line defect. Dark line defects have been reported to produce chemical changes in the material also [65]. These type of defects and degradation are often associated with increases in the threshold current density of the laser as well as decreased efficiency.

Other degrading factors include diffusion from the electrodes of the device and solders that are used in mounting the device. Diffusion of metals can cause paths of lower resistance which in turn leads to uneven current distribution in the device. The increased local current density lowers efficiency and promotes further generation of defects. Device degradation following these phenomena is often very rapid. [64]

Testing of life times of laser diodes requires a statistical approach. Often the minimal number of devices tested to produce reliable data is in the order of hundreds. Laser devices in testing can be operated either by constant current density in which case the output power will decrease over time or by maintaining a certain output power which means the input current must be increased over time [66]. Either way, the device is operated in controlled temperature with constant output power or input current. The output power of the laser is recorded in certain intervals to notice degradation or failure of the device.

Depending on the purpose of the laser, its operating conditions might be very low optical output powers and can lead to device life time test of continuous operation as long as 3 years [67]. Because of this it is sometimes desirable to simulate harsher conditions for the laser. This is especially useful in situations where the main failure modes of the devices are dependent on the operating temperature and thus can be thermally accelerated [64]. Measuring life time with increased operating current and optical output power does not often produce relevant results as these conditions are easily prevented in normal operation.

5. RESULTS AND ANALYSIS

5.1 Parametrization of the assist source

The goal for first part of measurements was to parametrize the assist source of the ion beam sputter. The parameters that were to be varied were the power of the RF coil of the assist source as well as the positive voltage. The initial plan to do this was to use glass monitor pieces with 56 nm of TiO_2 and 493 nm of Al_2O_3 coated on top of them. This kind of coating was used to see distinguishable features in the transmission spectrum measured by the optical monitoring system of the coater. By inserting a pre-coated monitor piece to the coater, it can be exposed to the assist source and the optical monitoring system can be used to solve the remaining coating on the monitor piece and thus etching speed of the assist source. The benefit of this kind of testing is that multiple parameter combinations can be tested in one run without venting the coating chamber.

Usage of glass monitor pieces to determine the etching speed of certain set of parameters had a significant problem. During long measurement runs the assist source sputtered material from the roof of the coating chamber to the backside of the glass monitoring piece. The material that was sputtered to the backside was not transparent and led to dramatic decrease in the transmission levels. As the changes in the thickness of the Al_2O_3 layer on the monitor pieces must be of the order of tens of nanometers that the changes in the spectrum can be accurately analyzed, this lead to the fact that only few parameters could be tested before the overall transmission drops enough to make the data impossible to analyze.

The problem of backside coating lead to an understanding that the vertical position of the substrate holder, shown in Fig. 11, was not optimal for the use of the assist source. Backside coating is only significant when a large portion of the ion beam misses the substrate holder and hits the roof of the chamber instead. The method for optimizing the vertical position of the substrate was also decided to be different. This was because the position of the substrate holder was decided to be optimized not only as a function of the intensity of the ion beam in a specific spot of the holder but also as a function of the uniformity around the same spot. 90 mm long slabs of silicon were coated with roughly 100 nm of Al_2O_3. Various positionss were tested for the substrate holder. The assist source was operated with 140 W power at the RF coil, further on referenced as RF power, 1000 V positive voltage, 800 V negative voltage and operating gases were 10 sccm of argon and 10 sccm of hydrogen. Ellipsometer was used to measure the thickness of Al_2O_3 before and after the exposure to determine the amount of etched material. Visibility of the ion beam made it possible to roughly place the substrate holder at the right position. Results of etching on various positions are showed in Fig. 15.

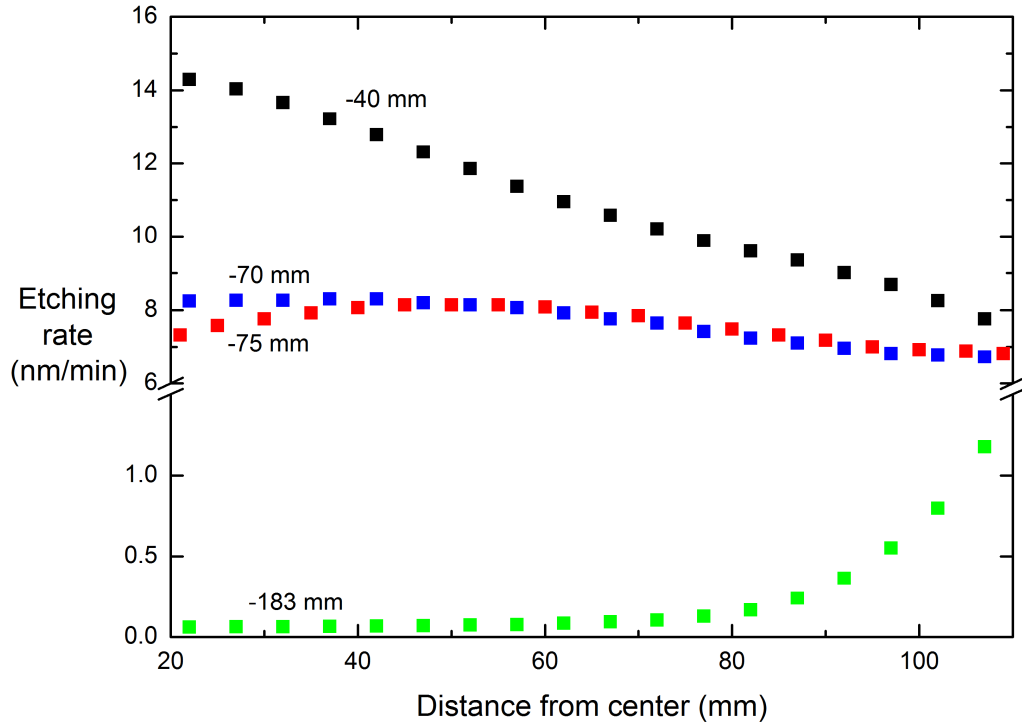

Figure 15. *Etching patterns of the assist source at various positions of substrate holder. At initial position of –183 mm very little of the beam hit the substrate holder at all.*

Adjustment of the substrate holder position to –75 mm had a tremendous effect on the effectiveness of assist source in terms of etching speed and yielded an even enough etching pattern. Position –40 mm resulted in faster etching over the whole region but was not as uniform. –70 mm was also a potential position but –75 mm had slightly better uniformity near the location 75 mm, where the samples are placed.

Assist source parametrization in terms of RF power and positive voltage was also done using the same method as in position optimization. Some combinations of parameters voltages resulted in unstable operation of the assist source. This often happened when positive voltage was lowered significantly but RF power was kept high. The effect of this was that the beam did not focus properly. To some degree the problem could be fixed by turning the assist source on with more stable parameters and only then changing the parameters to desired values. Etching patterns of various parameter combinations are plotted in Fig. 16. All the parameter combinations shown in Fig. 16 resulted in stable and properly focused beam.

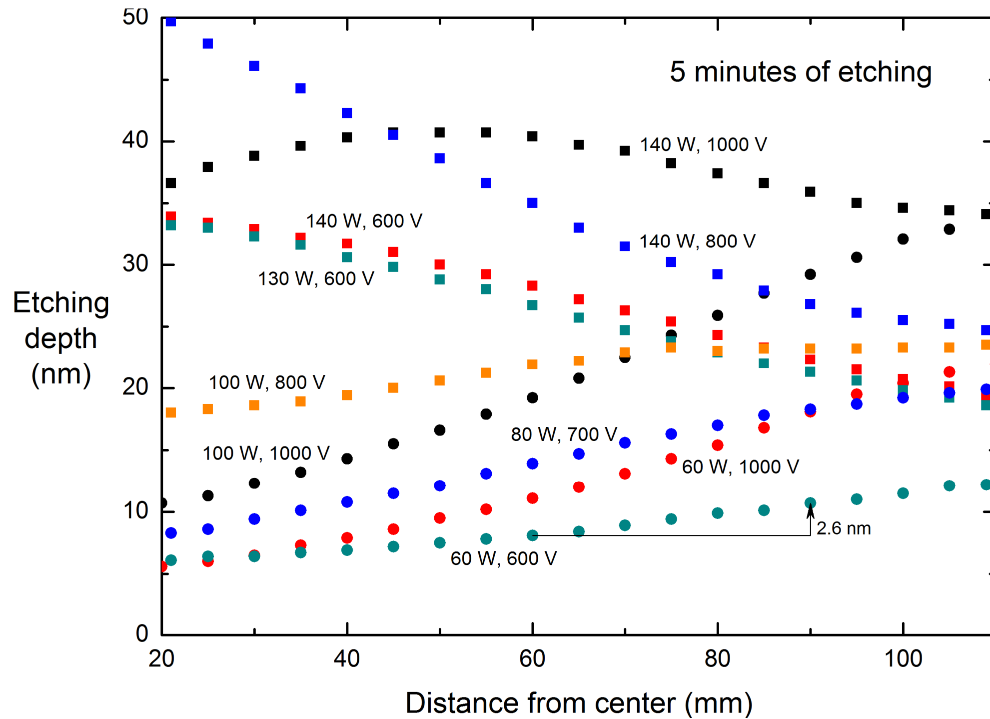

Figure 16. *Etching patterns of the assist source for various combinations of RF power and positive voltage. Etching time for every combination was 5 min, negative voltage 800 V and operating gases were 10 sccm of argon and 10 sccm of hydrogen. For parameters 60 W, 600 V the amount etched changed only 2.6 nm between 60 mm and 90 mm, resulting in good uniformity. Sample height of –75 mm was used.*

As can be expected, independently lowering either the positive voltage or RF power generally results in a lower etching rate. However, the position for the most etching seems to vary heavily depending on the positive voltage and RF power used. In some cases like lowering the positive voltage from 1000 V to 800 V with 140 W RF power leads to deeper etching near the center of the substrate holder. If the etching pattern is to be kept uniform, the RF power and positive voltage need to be lowered in tandem. RF power of 60 W and positive voltage of 600 V were chosen for cleaning treatment as it resulted in good uniformity as well as lowest etching speed.

Assist source was also tested with operating gases of 10 sccm of nitrogen and 10 sccm of hydrogen. Parameter combinations 60 W, 600 V and 80 W, 700 V were tested as before using only different gas combination. Results compared to respective parameters with argon and hydrogen gas combination can be seen in Fig. 17. The change in operating gases caused the etching speed to drop significantly. The result is expected as replacing the heavy argon atoms with lighter nitrogen lowers the etching capabilities of the ion beam.

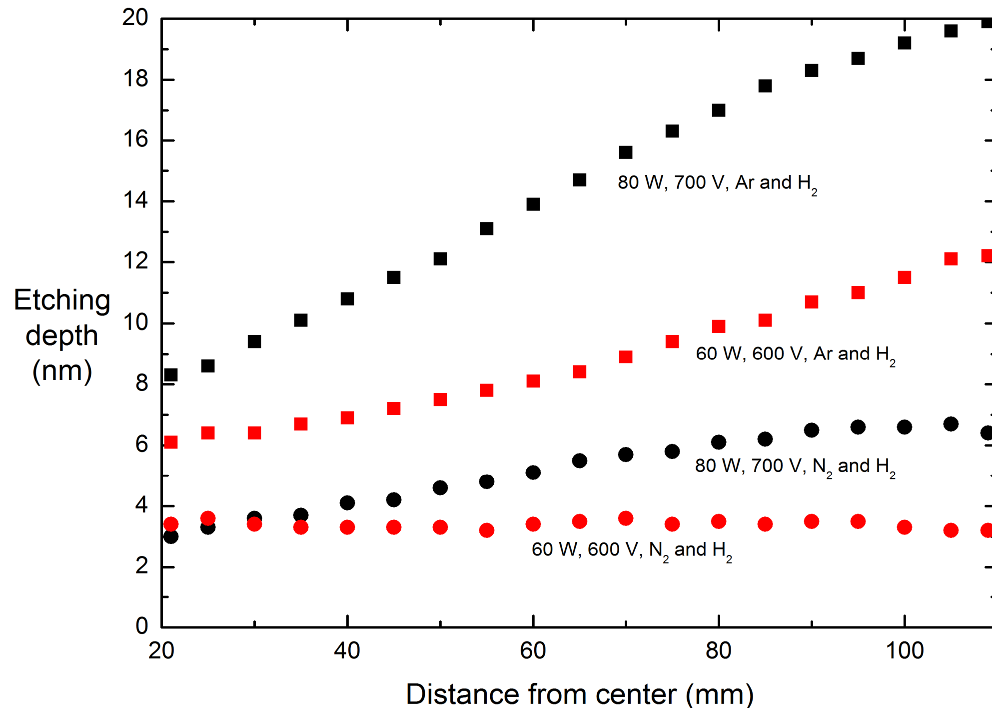

Figure 17. *Comparison of etching profiles for two different gas combinations. Replacement of argon with hydrogen results in a significantly lower etching rate and good uniformity.*

Parametrization was done for deposition parameters of silicon nitride using IAD. Primary source was operated with 115 W RF power, 1500 V positive voltage, 1200 V negative voltage and 8 sccm of argon. Position of the substrate holder was –75 mm. RF power and positive voltage was again varied for the assist source to find parameters that implement enough nitrogen into the deposited silicon but does not etch faster than silicon is deposited.

RF power of 150 W, 420 V positive voltage, 800 V negative voltage and 20 sccm of nitrogen were used to produce silicon nitride. The quality and thickness of the deposited silicon nitride varied depending on the position at the substrate holder. Refractive index of the silicon nitride varied between 1.929 and 1.968 between distances of 65 mm and 85 mm from center of the substrate holder. Similarly the thickness of the silicon nitride film varied 65.1 nm to 75.1 nm. At the position of 75 mm, the deposition rate for silicon nitride was 3.81 nm/s with the refractive index of 1.953.

5.2 Testing of surface treatments

Parametrization of the assist source was used perform treatments to semiconductor diode lasers. The standard treatment was designed so that 1.5 nm oxide layer could be removed with the cleaning treatment and a passivating 10 nm thick layer of silicon nitride is deposited on top of the cleaned surface. Argon and hydrogen were used as working gases for the standard cleaning treatment. Longer cleaning times as well as a design with a silicon passivation layer, cleaning treatment with nitrogen and hydrogen as working gases and tantalum AR coating was also tested. Both AR and HR facets were treated unless otherwise stated. Design of DBR mirror for HR facet remained constant. 4-pair DBR structure of silicon oxide and titanium oxide pairs was used with the first low index layer being an aluminum oxide layer. AR coating design was a standard aluminum oxide one layer AR in all other designs except when the tantalum AR was used. All the devices were 2 mm long with 100 µm emitter width. Table 1 shows the operating parameters for both primary and assist source treatments done.

Table 1. *Ion source parameters used for treatments. Treatment C is mentioned twice as it uses both sources.*

Symbol		**A**	**B**	**C**	**D**	**E**	**C**	**F**	**G**
Ion source		Assist source					Primary source		
Treatment type	**-**	Argon and hydrogen cleaning	Argon and hydrogen cleaning	Argon and hydrogen cleaning	10 nm sili-con nitride passivation	Nitrogen and hydro-gen cleaning	10 nm sili-con nitride passivation	Tantalum oxide AR coating	10 nm sili-con pas-sivation
Treatment length	**s**	64	300	600	157	120	157	-	90
RF power	**W**	60	60	60	150	60	115	150	115
Positive voltage	**V**	600	600	600	420	600	1500	2000	1500
Negative voltage	**V**	800	800	800	800	800	1200	600	1200
Ar flow	**sccm**	10	10	10	0	0	8	8	8
H2 flow	**sccm**	10	10	10	0	10	0	0	0
N2 flow	**sccm**	0	0	0	20	10	0	0	0
O2 flow	**Sccm**	0	0	0	0	0	0	5	0

The treated chips were mounted to submounts and tested with a COD setup. The setup included a pulse driver that could produce 2 µs pulses with a 1 % duty cycle. Increase of power was done by a program that increased the current automatically after stabilization time of 2 s. Power was measured using an integrating sphere. It is important to note that the pulse is not a perfect tophat shape and the peak power is a calculated estimate from average measured power and duty cycle. Spectral data was gathered also during measurement. COD levels for laser chips with various treatments are shown in Fig. 18.

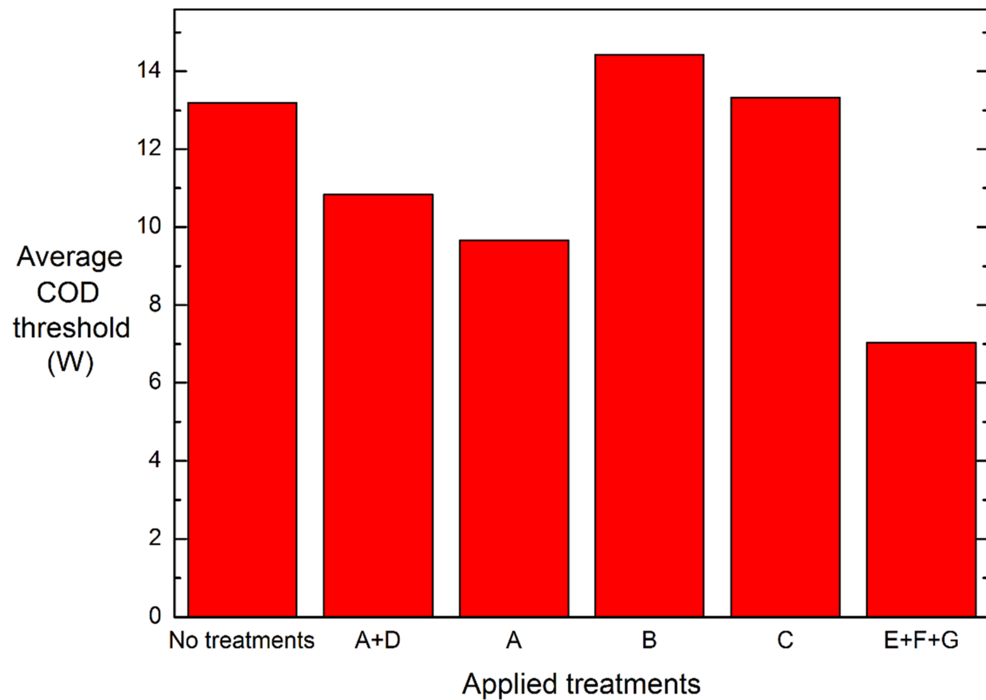

Figure 18. *Average COD levels for laser chips with various treatments. Description and parameters used for each treatment can be found in Table 1. One non-treated and one chip from treatment C did not experience COD.*

Applying the standard cleaning and passivation treatment lowered the average COD level by almost 20 %. Even worse COD threshold was observed when only the 1 minute cleaning treatment was applied. When the cleaning treatment length was increased to 5 and 10 minutes the COD threshold increased slightly. The design with silicon passivation, cleaning with nitrogen and hydrogen and tantalum AR coating resulted in drastically lowered COD thresholds. 2 chips, one non-treated and one with 10 minute argon and hydrogen cleaning, did not experience COD during the measurement.

According to the results there are problems with both the cleaning treatment and silicon nitride passivation. One possible explanation for the weakened performance of the devices that were cleaned for 1 minute is that all of the harmful oxides were not removed during the cleaning treatment. As the facet suffers some mechanical damage during the cleaning treatment it is possible that 1 minute of cleaning only roughens up the surface without implementing the actual benefits of the cleaning. 5 minutes of cleaning resulted in the best COD threshold. 10 minutes of cleaning caused visible height differences to be

seen in the AR facet as the different materials in epilayers etch at different rates. This irregularity at the laser facet is likely to lower the COD threshold.

The AR facets of the devices were photographed with a microscope before and after testing. This was done to screen out failures such as contamination or physical damage suffered by the AR coating. Vast majority of samples showed clear black lines and dots at the emitter, indicating optically caused damage at the AR coating or at its immediate proximity.

General effect of the applied treatments was that COD level of the devices decreases. Also, when compared to a commercial coating the overall COD threshold of the samples, including the reference sample that was only coated, is notably lower. This is a clear indicator that other parts of the coating process are also factors that lower the COD threshold.

5.3 Effect of primary source deposition parameters

Comparison of the deposition rates for materials used in coatings showed that the IBS coater used in this thesis deposits the layers faster than other coaters. This indicated that the main reason for previously seen lowered COD thresholds could be caused due to too high parameters of the primary source. Different positive voltages and RF powers were tested specifically for depositing aluminum oxide layer. This is because the first layer of both designs are aluminum oxide. It was also supposed that the parameters for growing other layers of the DBR did not matter as much as the first aluminum oxide layer is thick enough to prevent ion implementation and other harmful effects. The deposition rate of aluminum oxide was changed so that both the RF power and positive voltage of the primary source were multiplied with a certain number, called parameter factor. Original positive voltage and RF power in the recipe were 1800 V and 145 W respectively. Devices were from the same structure as the devices in Fig. 18. COD thresholds for not cleaned or passivated devices with aluminum oxide layers coated with different parameter factors are showed in Fig. 19.

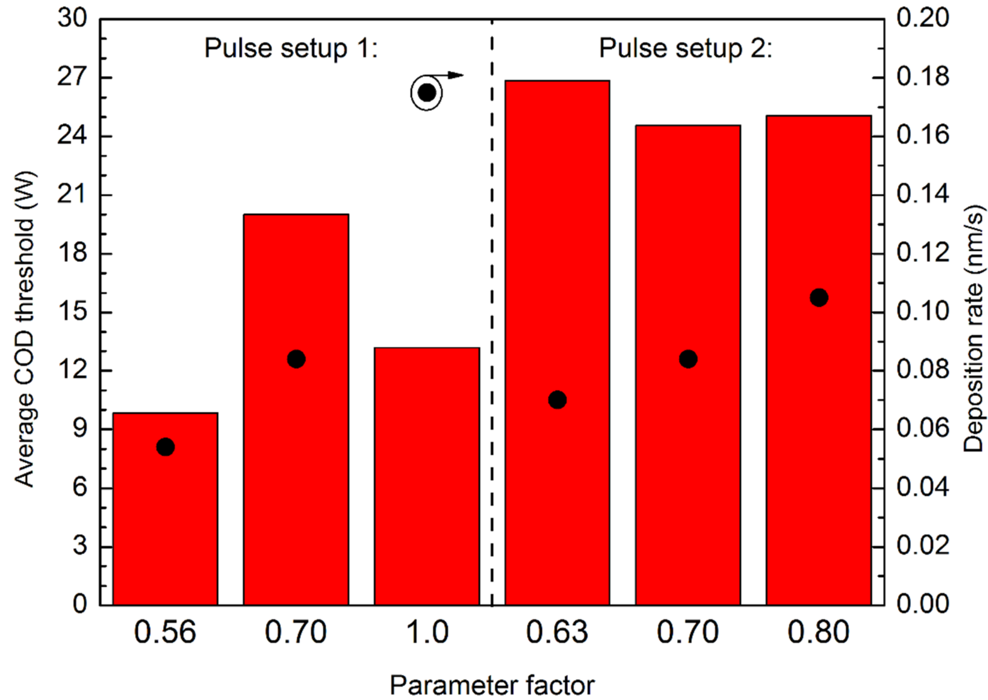

Figure 19. *COD thresholds for laser chips with varied parameter factors for aluminum oxide deposition. Different pulse setup was used for chips in the right part of the figure as 0.70 parameter factor chips did not experience COD when operated with the 30 A pulse setup. Average COD thresholds are demonstrated in the left y-axis as the reed columns while the deposition rate for each parameter factor is shown as the black dot and the corresponding values are on the right y-axis.*

Changing the deposition rate of aluminum oxide had a formidable effect on the device COD threshold. Deposition rate of 0.054 nm/s obtained with the power factor 0.56 caused the average COD threshold of the devices to drop to 9.84 W. Similarly, using the original parameters, the average COD threshold of the devices is only 13.2 W. Usage of parameter factor of 0.70 resulting in 0.084 nm/s deposition rate caused majority of the devices to be robust enough to survive the maximum output of the pulse driver setup resulting in demonstrated average COD threshold of at least 20 W. This improvement is so large that it is very likely that the earlier demonstrated passivation layers cause similar damage to laser facets if their deposition parameters are not corrected.

Parameter factors of 0.63, 0.70 and 0.80 were further tested with more powerful pulse driver, resulting in COD thresholds of 26.9 W, 24.6 W and 25.1 W. The best parameter factor was 0.63 while 0.7 yielded the lowest average. The RF power and positive voltage for 0.63 parameter factor are 91 W and 1134 V respectively. The slightly weaker performance of the chips coated with 0.70 parameter factor is likely explained due the fact that the chips were already once tested in the first part of the measurements. The first layer of the DBR structure at HR facet for 0.70 chips was not deposited with the corrected parameters which may have affected the result also. However, it is likely that if the HR side

deposition rate affected the COD threshold, it would lower the COD threshold significantly rather than by a miniscule amount. It is imperative to note that the pulse shape and other factors change when different pulse setup is used. This means that comparative analysis can only be done between CODs measured with the same setup and absolute differences in COD thresholds cannot be derived between setups.

Too low deposition rates are known to cause high concentration of impurities in coatings. This is because some amount of impurities are always present in the coating chamber and if the deposition rate is lowered enough, more impurities have time to implement in the coating. On the other hand, too high a deposition rating causes the quality of the deposited material to decrease. This is known to happen by layers indicating increased stress as well as uneven deposition of the material, resulting in imperfections inside the layers making the layer more porous. These known phenomena are likely to affect the quality of the aluminum oxide layer enough to contribute to the differences in COD thresholds.

Ion implementation during sputtering affects the device negatively. As too energetic ions hit the target material, also the coating material sputtered from the target will have high energy. This causes damage to the crystal structure and can also be used to explain the lowered COD threshold of the samples coated with high parameter factor. When the parameter factor is lowered, and the energy of the ions decrease below the energy that is required to detach an atom for the target, the sputtering atom can bounce from the material target's surface without losing much energy as it cannot break the chemical bonds at the target. These ions can reach the laser facet with high energy and cause damage to the semiconductor lattice.

5.4 Future possibilities

Optimization of aluminum oxide sputtering parameters improved the COD threshold of the laser diodes tremendously. Similar optimization could be done to other materials, namely tantalum oxide as it is used in AR coatings. It is also of interest to test what causes the improvement in the coating COD threshold when the parameters are optimized. This could be tested by independently lowering the RF power and positive voltage. Testing this could yield insight to if ion implementation to the semiconductor, stress properties of the thin films or perhaps something else is causing the lower COD thresholds of the coated device.

The primary source parameters for passivation treatments should also be optimized. This if wrong parameters, namely too high ion energy, is causing the tendency for low COD thresholds, it will also happen during evaporation of passivation layers which involve sputtering. A natural continuum would then be the testing of a new set of assist source

treatments for devices with the already optimized primary source parameters. It is reasonable to assume that the cleaning and passivation treatments would have a different effect had the primary source parameters been more optimal.

Some tracks of different type of treatments could be tested out. For example, the nitrogen-based cleaning treatments, which could clean and passivate at the same time, were not extensively tested. It might be beneficial to also lower the cleaning treatment RF powers and positive voltages to experiment with even gentler treatments. Also, different passivation treatments such as silane compounds were left untested. The vast amount of possible different treatments result in a myriad of treatment combinations that have to be tested if one wants to optimize the surface treatment of semiconductor diode laser.

6. CONCLUSIONS

Assist source was successfully parametrized for steady operation uniform etching at rates as low as 1 nm/min. Parameters for silicon nitride deposition using IAD were also found. Laser devices treated with different treatment combinations resulted in average COD thresholds between 7.0 and 14.0 W. The applied cleaning and passivation treatments had a negative influence on laser COD threshold excluding the 5 and 10 minute argon based cleaning treatments, which increased the COD threshold by 9 % and 1 % respectively. Average COD threshold of the non-treated reference devices was 13.2 W. Taking into account the margins of error originating from mainly the pulse setup, this level of effect does not indicate importance of the cleaning. Effect of the cleaning and passivation treatments are inconclusive as the initial deposition parameters for aluminum oxide were the root cause of the low COD thresholds.

Tuning the deposition parameters of aluminum oxide in AR coating and in the first layer of DBR layer structure at HR had a significant effect on device COD threshold. When the sputtering of aluminum was done either with too high or too low ion energy, the COD threshold decreases. Significant improvement in COD threshold was measured when parameter factors 0.63, 0.70 and 0.80 were used. Highest average COD threshold of 26.9 W was measured when 0.63 parameter factor was used. RF power and positive voltage for 0.63 corresponds to 91 W and 1134 V, respectively. Usage of 0.63 parameter factor resulted in at least 50 % increase in average COD threshold in measured laser devices.

REFERENCES

[1] R. N. Hall, G. E. Fenner, J. D. Kingsley, T. J. Soltys, and R. O. Carlson, “Coherent light emission from GaAs junctions,” *Phys. Rev. Lett.*, vol. 9, no. 9, pp. 366–368, 1962.

[2] F. A. Smidt, “Use of ion beam assisted deposition to modify the microstructure and properties of thin films,” *Int. Mater. Rev.*, vol. 35, no. 1, pp. 61–128, 1990.

[3] G. Busch, “Early history of the physics and chemistry of semiconductors - from doubts to fact in a hundred years,” *Eur. J. Phys.*, vol. 10, pp. 254–264, 1989.

[4] L. Łukasiak and A. Jakubowski, “History of Semiconductors,” *J. Telecommun. Inf. Technol.*, vol. 1, no. IS, pp. 3–9, 2010.

[5] U. K. Mishra and J. Singh, *Semiconductor Device Physics and Design*. Springer Science & Business Media, 2008.

[6] B. Van Zeghbroeck, “Principles of Semiconductor Devices,” 2011. [Online]. Available: https://ecee.colorado.edu/~bart/book/book/chapter2/ch2_2.htm. [Accessed: 08-Dec-2017].

[7] S. Lei *et al.*, “Evolution of the electronic band structure and efficient photo-detection in atomic layers of InSe,” *ACS Nano*, vol. 8, no. 2, pp. 1263–1272, 2014.

[8] M. Riordan and L. Hoddeson, “Origins of the p-n junction,” *IEEE Spectr.*, vol. 34, no. 6, pp. 46–51, 1997.

[9] N. C. C. MacDonald and T. E. E. Everhart, “Direct measurement of the depletion layer width variation vs applied bias for a p-n junction,” *Appl. Phys. Lett.*, vol. 7, no. 10, pp. 267–269, 1965.

[10] R. Nave, “HyperPhysics,” *P-N junction*, 2000. [Online]. Available: http://hyperphysics.phy-astr.gsu.edu/hbase/Solids/pnjun.html. [Accessed: 23-Dec-2017].

[11] S. L. L. Sheng, “pn Junction Diodes,” in *Semiconductor Physical Electronics*, no. 1, 2006, pp. 334–380.

[12] W. W. Gärtner, “Depletion-layer photoeffects in semiconductors,” *Phys. Rev.*, vol. 116, no. 1, pp. 84–87, 1959.

[13] Nikhil M.R, “Engineering 360,” *Diodes Information*, 2017. [Online]. Available: http://www.globalspec.com/learnmore/semiconductors/discrete/diodes/diodes_all_types. [Accessed: 30-Dec-2017].

[14] T. Tokuyama, “Zener breakdown in alloyed germanium p-n junctions,” vol. 5, pp. 161–169, 1962.

[15] C. Zener, “A Theory of the Electrical Breakdown of Solid Dielectrics,” vol. 145, no. 855, pp. 523–529, 2014.

[16] K. G. McKay and K. B. McAfee, “Electron multiplication in silicon and germanium,” *Phys. Rev.*, vol. 91, no. 5, pp. 1079–1084, 1953.

[17] S. T. Tan, X. W. Sun, H. V. Demir, and S. P. Denbaars, “Advances in the LED materials and architectures for energy-saving solid-state lighting toward lighting revolution,” *IEEE Photonics J.*, vol. 4, no. 2, pp. 613–619, 2012.

[18] A. Aho *et al.*, “Composition dependent growth dynamics in molecular beam epitaxy of GaInNAs solar cells,” *Sol. Energy Mater. Sol. Cells*, vol. 124, pp. 150–158, 2014.

[19] H. Gerischer, “Electrochemical photo and solar cells principles and some experiments,” *J. Electroanal. Chem.*, vol. 58, no. 1, pp. 263–274, 1975.

[20] A. Gubanov, V. Polojärvi, A. Aho, A. Tukiainen, N. V. Tkachenko, and M. Guina, “Dynamics of time-resolved photoluminescence in GaInNAs and GaNAsSb solar cells,” *Nanoscale Res. Lett.*, vol. 9, no. 1, pp. 1–4, 2014.

[21] G. P. Weckler, “Operation of p-n Junction Photodetectors in a Photon Flux Integrating Mode,” *IEEE J. Solid-State Circuits*, vol. 2, no. 3, pp. 65–73, 1967.

[22] O. N. Acosta, “Zener diode-a protecting device against voltage transients,” *IEEE Trans. Ind. Gen. Appl.*, vol. I, no. 4, pp. 481–488, 1969.

[23] “The Nobel Prize in Physics 1956.” [Online]. Available: https://www.nobelprize.org/nobel_prizes/physics/laureates/1956/. [Accessed: 24-Jan-2018].

[24] A. Einstein, “Zur quantentheorie der strahlung,” *Phys. Z.*, pp. 121–128, 1917.

[25] T. H. Maiman, “Optical maser action in ruby,” *Adv. Quantum Electron.*, 1961.

[26] H. Liang and J. Lawrence, *Laser surface treatment of bio-implant materials*. Wiley UK, 2005.

[27] K. Kincade, A. Nogee, G. Overton, D. Belforte, and C. Holton, “Annual Laser Market Review & Forecast: Lasers enabling lasers,” 2018. [Online]. Available: http://www.laserfocusworld.com/articles/print/volume-54/issue-01/features/annual-laser-market-review-forecast-lasers-enabling-lasers.html. [Accessed: 03-Feb-2018].

[28] R. Nave, “HyperPhysics,” *Stimulated Emission*. [Online]. Available: http://hyperphysics.phy-astr.gsu.edu/hbase/mod5.html. [Accessed: 03-Feb-2018].

[29] A. Y. Cho and J. R. Arthur, “Molecular beam epitaxy,” *Prog. Solid State Chem.*, vol. 10, no. PART 3, pp. 157–191, 1975.

[30] G. Feak *et al.*, “The Influence of Strain on the Small Signal Gain and Lasing Threshold of GaInAs/GaAs and GaAs/GaInAlAs Strained Layer Quantum Well

Lasers," *IEEE/Cornell Conf. Adv. Concepts*, pp. 362–372, 1989.

[31] E. Selcuk, "Guided and deterministic self organization of quantum dots," *TU/e PhD thesis*, 2009.

[32] R. Paschotta, "Laser Diodes," *Encyclopedia of Laser Physics and Technology*. [Online]. Available: https://www.rp-photonics.com/laser_diodes.html. [Accessed: 11-Feb-2018].

[33] R. Paschotta, "Edge-emitting Semiconductor Lasers," *Encyclopedia of Laser Physics and Technology*. [Online]. Available: https://www.rp-photonics.com/edge_emitting_semiconductor_lasers.html. [Accessed: 20-Jun-2018].

[34] W. Chow, S. Koch, and M. Sargent, *Semiconductor-Laser Physics*. Springer Science & Business Media, 2012.

[35] P. Savolainen, M. Toivonen, S. Orsila, and M. Saarinen, "AlGaInAs / InP Strained-Layer Quantum Well Lasers at 1 . 3 μ m Grown by Solid Source Molecular Beam Epitaxy," vol. 28, no. 8, pp. 980–985, 1999.

[36] R. Paschotta, "Vertical Cavity Surface-emitting Lasers," *Encyclopedia of Laser Physics and Technology*. [Online]. Available: https://www.rp-photonics.com/vertical_cavity_surface_emitting_lasers.html. [Accessed: 12-Feb-2018].

[37] H. Kogelnik and C. V. Shank, "Stimulated emission in a periodic structure," *Appl. Phys. Lett.*, vol. 18, no. 4, pp. 152–154, 1971.

[38] J. Hastie *et al.*, "High power CW red VECSEL with linearly polarized TEM00 output beam.," *Opt. Express*, vol. 13, no. 1, pp. 77–81, 2005.

[39] H. Angus Macleod, *Thin-Film Optical Filters*, 4th ed. CRC Press, 2010.

[40] E. Ritter, "Optical film materials and their applications.," *Appl. Opt.*, vol. 15, no. 10, pp. 2318–27, 1976.

[41] L. Orsila, "Optical Thin Film Technology for Ultrafast Fiber Lasers," PhD thesis, Tampere University of Technology, Publication: 731, 2008.

[42] K. Rabinovitch and A. Pagis, "Multilayer antireflection coatings: theoretical model and design parameters," *Appl. Opt.*, vol. 14, no. 6, p. 1326, 1975.

[43] S. G. K. Pillai, R. M. Pillai, and A. D. Damodaran, "Ancient metal-mirror making in South India," *JOM*, vol. 44, no. 3, pp. 38–40, Nov. 1992.

[44] W. Contributors, "Reflectance," 2017. [Online]. Available: https://en.wikipedia.org/wiki/Reflectance. [Accessed: 03-Mar-2018].

[45] "U. S. Military grade specification for optical thin films MIL-F-48616," 1977.

[46] H. H. Gatzen, V. Saile, and J. Leuthold, *Micro and nano fabrication: Tools and*

processes. 2015.

[47] R. Scrivens, “Classification of Ion Sources,” *Cern Yellow Rep. Cern.*, pp. 9–26, 2014.

[48] W. L. Gardner *et al.*, “Ion optics improvements to a multiple aperture ion source,” *Rev. Sci. Instrum.*, vol. 52, no. 11, pp. 1625–1628, 1981.

[49] H. R. Kaufman, J. J. Cuomo, and J. M. E. Harper, “Technology and applications of broad-beam ion sources used in sputtering. Part I. Ion source technology,” *J. Vac. Sci. Technol.*, vol. 21, no. 3, pp. 725–736, 1982.

[50] M. I. Boulos, “The inductively coupled R.F. (radio frequency) plasma,” *Pure Appl. Chem.*, vol. 57, no. 9, pp. 1321–1352, 1985.

[51] I. Kaufman and Robinson, “Gridded Ion Beam Sources.” [Online]. Available: http://www.ionsources.com/PDF/Gridded_Ion_Brochure.pdf. [Accessed: 27-Apr-2018].

[52] J. M. E. Harper, J. J. Cuomo, and P. A. Leary, “Low energy ion beam etching,” *J. Electrochem. Soc.*, vol. 128, no. 5, pp. 1077–1083, 1981.

[53] S. Chhajed, M. F. Schubert, J. K. Kim, and E. F. Schubert, “Nanostructured multilayer graded-index antireflection coating for Si solar cells with broadband and omnidirectional characteristics,” *Appl. Phys. Lett.*, vol. 93, no. 25, pp. 15–18, 2008.

[54] F. Reinhard, B. Dwir, and E. Kapon, “Oxidation of GaAs/AlGaAs heterostructures studied by atomic force microscopy in air,” *Appl. Phys. Lett.*, vol. 68, pp. 3168–3170, 1995.

[55] A. Goetzberger, V. Heine, and E. H. Nicollian, “Surface states in silicon from charges in the oxide coating,” *Appl. Phys. Lett.*, vol. 12, no. 3, pp. 95–97, 1968.

[56] M. B. Cosar, A. E. S. Ozhan, and G. H. Aydogdu, “Improving the laser damage resistance of oxide thin films and multilayers via tailoring ion beam sputtering parameters,” *Appl. Surf. Sci.*, vol. 336, pp. 34–38, 2015.

[57] T. Lauinger, J. Schmidt, A. G. Aberle, and R. Hezel, “Record low surface recombination velocities on 1 cm p-silicon using remote plasma silicon nitride passivation,” *Appl. Phys. Lett.*, vol. 68, no. 9, pp. 1232–1234, 1996.

[58] A. G. Aberle and R. Hezel, “Progress in Low-temperature Surface Passivation of Silicon Solar Cells using Remote-plasma Silicon Nitride,” *Prog. Photovoltaics Res. Appl.*, vol. 5, no. September 1996, pp. 29–50, 1997.

[59] H.-C. Chin, M. Zhu, G. S. Samudra, and Y.-C. Yeo, “n-Channel GaAs MOSFET with TaN/HfAlO Gate Stack Formed Using In Situ Vacuum Anneal and Silane Passivation,” *J. Electrochem. Soc.*, vol. 155, no. 7, p. H464, 2008.

[60] M. Ziegler *et al.*, “Catastrophic optical mirror damage in diode lasers monitored during single-pulse operation,” *Appl. Phys. Lett.*, vol. 94, no. 19, pp. 92–95, 2009.

[61] C. L. Walker, A. C. Bryce, S. Member, and J. H. Marsh, "Improved Catastrophic Optical Damage Level From Laser With Nonabsorbing Mirrors," vol. 14, no. 10, pp. 1394–1396, 2002.

[62] R. W. Lambert *et al.*, "Facet-passivation processes for the improvement of Al-containing semiconductor laser diodes," *J. Light. Technol.*, vol. 24, no. 2, pp. 956–961, 2006.

[63] S. L. Yellen *et al.*, "Reliability of GaAs-Based Semiconductor Diode Lasers: 0.6–1.1 µm," *IEEE J. Quantum Electron.*, vol. 29, no. 6, pp. 2058–2067, 1993.

[64] M. Ott, "Capabilites and Reliability of LEDs and Laser Diodes," *Intern. NASA Parts Packag. Publ.*, 1996.

[65] B. Foran, N. Presser, Y. Sin, M. Mason, and S. C. Moss, "Two Distinct Types of Dark-Line Defects in a Failed InGaAs / AlGaAs Strained Quantum Well Laser Diode," *Development*, pp. 4–5, 2009.

[66] J. Jiménez, "Laser diode reliability: Crystal defects and degradation modes," *Comptes Rendus Phys.*, vol. 4, no. 6, pp. 663–673, 2003.

[67] M. Fukuda, "Laser and Led Reliability Update," *J. Light. Technol.*, vol. 6, no. 10, pp. 1488–1495, 1988.